Srinivasan, G. R.: *J. Electrochem. Soc.*, vol. 127, p. 1334, 1980.
Taniguchi, K., Kurosawa, and M. Kashiwagi: *J. Electrochem. Soc.*, vol. 127, p. 2243, 1980.
Townsend, P. D., J. C. Kelly, and N. E. W. Hartly: *Ion Implantation, Sputtering and Their Applications*, Academic Press, 1976.
Tsai, J. C. C.: in S. M. Sze (ed.), *VLSI Technology*, chap. 5, McGraw-Hill, New York, 1983.
———, F. F. Morehead, and J. E. E. Baglin: *J. Appl. Phys.*, vol. 51, p. 3230, 1980.
Tuck, B.: *Introduction to Diffusion in Semiconductors*, vol. 16, p. 119, IEE Monograph Services, London, 1974.
Webber, R. F., R. S. Thorm, and L. N. Large: *Int. J. Electronics*, vol. 26, p. 163, 1969.
Yeh, T. H., and W. Armstrong: Electrochemical Society Meeting, Abstract 69, Indianapolis, Spring 1961.

CHAPTER 8

PATTERN GENERATION, TRANSFER, AND DELINEATION

8.1 LITHOGRAPHY

Design of an integrated circuit eventually leads to specification of the circuit elements in terms of the length, width, and depth of each element such as doped regions, isolated (insulated) regions, conducting regions, and so on. The "blueprint" containing the specifications and the layout of the device elements is referred to as composite layout. Elements overlay in the device structures considered in Chap. 1 (e.g., Fig. 1-13), so it is necessary to specify the order that overlaying elements are to be processed for device fabrication and also specify the patterns of the layout corresponding to each step of the fabrication.

The minimum number of patterns required for fabrication is the number of mask levels. Each level represents the mask that can be used to transfer the mask pattern to the wafer surface. Figure 8-1 shows a composite layout of a minimum geometry bipolar transistor (Colclaser, 1980). The corresponding mask levels are shown in Fig. 8-2 in the order to be fabricated. Note that the first mask level is for the mask defining the pattern for the buried layer, although the dimensions are not given. The masks in Fig. 8-2 are to the scale of the composite layout in Fig. 8-1. The second mask is for isolating the buried layer from the rest of the device structure to be fabricated by subsequent processing. An examination of all

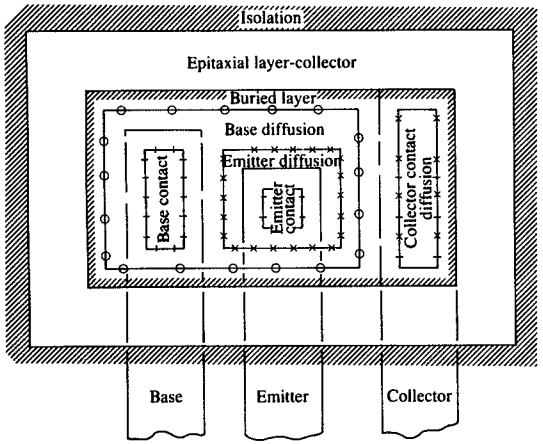

FIGURE 8-1
A composite layout of a minimum geometry bipolar transistor (Colclaser, 1980).

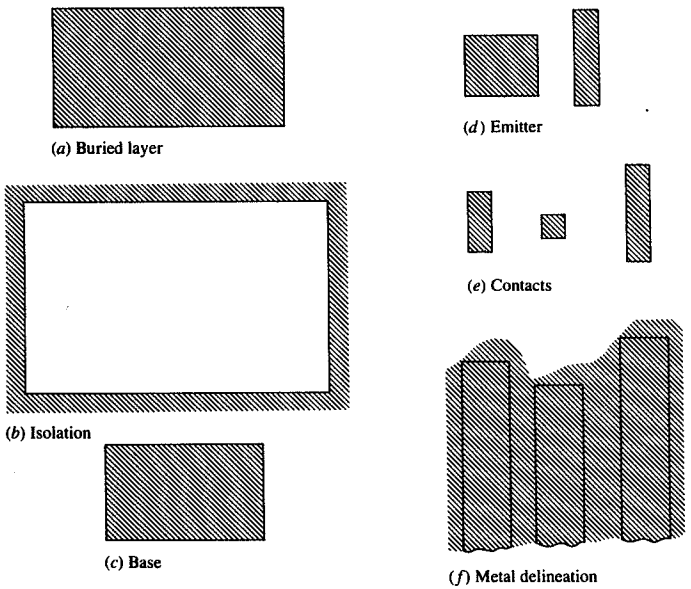

FIGURE 8-2
Individual masks for the transistor of Fig. 8-1 (Colclaser, 1980).

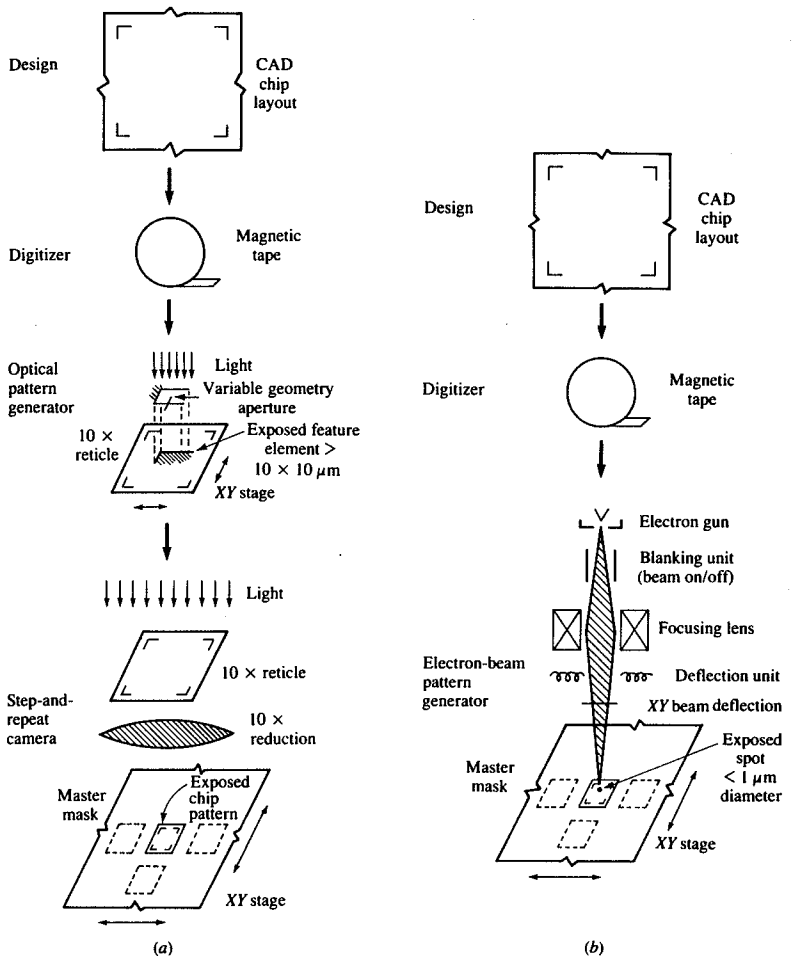

FIGURE 8-3
(*a*) Schematic representation of photolithographic mask fabrication; (*b*) e-beam method (Ballantyne, 1980).

the mask levels in Fig. 8-2 should reveal that the device fabrication proceeds, in general, from the lowest to the uppermost layer of the fabricated device, the uppermost being the metal delineation representing the metallization pattern.

The composite layout and the mask patterns were once made by drawing an oversized picture and then reducing the size successively by photographic

reduction to the actual miniature scale. Today computer-aided design (CAD) is used primarily with the aid of a software library to design the circuit on a CRT. Then the final design is digitized and stored on a tape to generate the composite layout and mask patterns. These patterns are registered on masks made from glass plates coated with either an emulsion or a hard film of chromium, chromium oxide, or silicon. The process of transferring a pattern onto a substrate, which can be a wafer or a mask material, is called lithography. The mask material of the coated glass plate with the transferred pattern is called a master mask or simply mask.

The mask can be fabricated by photolithographic or electron-beam (e-beam) methods. Schematic examples of the methods are shown in Fig. 8-3. The pattern is usually delineated either photographically, in high-resolution emulsion on glass plates, or photolithographically (Fig. 8-3*a*) on chromium films on glass plates. Both these and the e-beam methods involve the use of a resist. A resist is a material that is sensitive to either light or e-beam such that a pattern can be engraved into the resist film, in much the same way as conventional photographic development. Because of the poor resolution of lines inherent in thick emulsions (4 to 6 μm), chromium films are preferred. The mask fabrication is similar to the usual lithography involved in device fabrication. However, better resolution is afforded by the much thinner resist film and the absence of steps (thus planar surface) in the mask fabrication.

Although the resist is also used in the mask fabrication, the name is derived from the fact that the portion of the surface covered by the resist in device fabrication is protected from (resistant to) penetration of undesired materials to the protected surface, whether the penetration is by diffusion, chemical reaction, or ion implantation. Almost all resists are of a polymeric material, which upon sensitization by light, x-ray, or e-beam, changes its chemical structure in such a way that the sensitized portion either dissolves (positive resist) or remains intact (negative resist) when placed in a suitable solvent. These two types of resist are shown in Fig. 8-4, which illustrates the e-beam mask fabrication.

Once the masks are made, the resist material is spin-coated onto the wafer. Then the resist on the wafer is exposed to a sensitizing source through the mask so that the mask pattern is transferred onto the resist. The resist film thickness l resulting from the spin coating (Thompson and Bowden, 1983) is often correlated as follows:

$$l = \frac{KC^{\beta}\mu^{\gamma}}{S^{\alpha}} \tag{8.1}$$

where C is the concentration of the resist solution (percent solids), S is the spinning speed (r/min), K is a constant, μ is the viscosity on the polymeric material, and α, β, and γ are constants. The sensitized resist is then developed in a solvent so that the desired pattern emerges after the development for the actual device fabrication steps such as film deposition, ion implantation, and so on, that are specified by the mask and masking level. In essence, repetition of lithographic processing constitutes the entire device fabrication procedure as shown in Fig. 8-5. The portion within the box represents the processing steps for the lithography, each cycle representing one mask level. Each time the cycle is repeated, the new mask pattern has to be aligned to the pattern already present on the wafer.

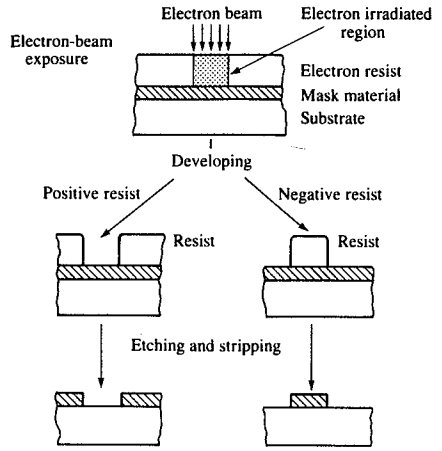

FIGURE 8-4
An e-beam mask fabrication process (Ballantyne, 1980).

An analysis of the growth trend in the number of components per chip over a 14-year period prior to 1975 (Moore, 1975) indicates an increase by a factor of 64,000, of which a factor of 32 was attributed to improvements in lithography, a factor of 20 to the use of larger chips, and the remaining factor of 100 to improved circuit design and layout. Obviously lithography has been a key to the miniaturization of integrated circuits. More important, however, the ultimate limitation to miniaturization, even when inherent limitations in device design are resolved, is the ability to clearly delineate high-resolution patterns by lithography.

Photolithography based on ultraviolet light (300 to 400 nm wavelength) has been the main lithography method and can deliver nearly 0.5 μm resolution under practical conditions. Electron beam lithography, which is typically being used for mask fabrication, is likely to be the main means by which practical lithography is carried out in the future. Lithography based on soft x-rays (0.1 to 5 nm wavelength), which almost eliminates the diffraction effects that limit the resolution in photolithography, suffers from poor contrast and low energy but could fill the gap between photolithography and e-beam lithography. The major problem in e-beam lithography is electron scattering. This has led to lithography based on ions or ion-beam lithography. Although there are still major problems yet to be solved, it has already been demonstrated in laboratory work that 10 nm resolution is possible even with e-beam.

The basics governing the various lithographies are very complex. Nevertheless, an understanding of some basics of optics and particle beams, theoretical and approximate, is needed for subsequent chapters. These principles are treated next.

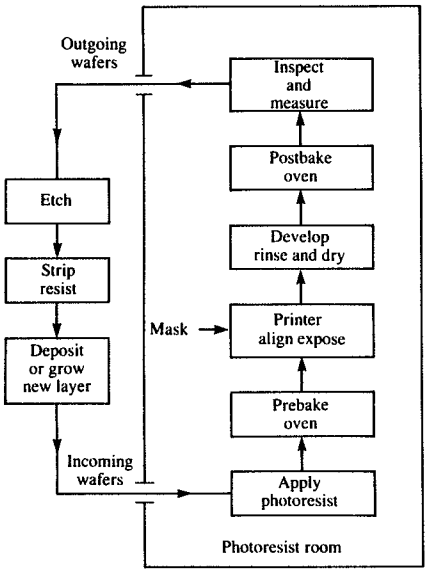

FIGURE 8-5
Lithographic processing sequence (McGillis, 1983).

8.2 BASICS OF OPTICS AND PARTICLE BEAMS

When a beam of light strikes a flat, shiny surface (a plane mirror), it is reflected. The law of reflection is that the incidence angle (the angle between the incident beam and a line normal to the mirror surface) is equal to the reflection angle (the angle between the reflected beam and the normal line). Light also travels through a transparent material. When a beam of light enters a transparent material at an oblique angle to its surface, the phenomenon of refraction occurs, i.e., bending of the beam. This is due to the fact that the light always travels in a material at a speed less than the speed of light in vacuum. A measure of this speed is called the refractive index n:

$$n = \frac{C}{v} \tag{8.2}$$

where C is the speed of light in vacuum and v is the speed of light in the transparent material. The law of refraction or Snell's law states that when a light beam passes from one medium (with refractive index n and incidence angle Ω) to another (with refractive index n' and refraction angle Ω', which is the angle between the refractive beam and a line normal to the interface), it satisfies the following relationship:

$$n \sin \Omega = n' \sin \Omega' \tag{8.3}$$

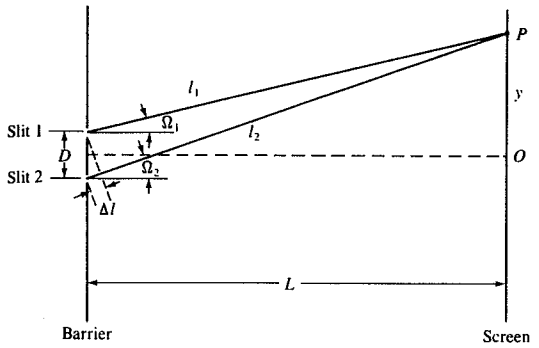

FIGURE 8-6
Two-slit diffraction behavior (Eisberg and Lerner, 1981).

The most important optical behavior in photolithography is diffraction, the phenomenon of bending around corners due to the wave property of light. Consider the diffraction pattern that results when a light beam passes through two slits in a barrier, as shown in Fig. 8-6. The light travels to the right with speed v and wavelength λ. The wavelength is the distance between two crests with a trough in between in a wave. As the light wave passes through the two slits, it diffracts. Consider two particular components of the diffracted beam out of the two slits, one reaching the point P and another reaching the point O on the screen in Fig. 8-6. The diffracted beam out of the slit 1 that reaches the point O travels the same distance as that out of the slit 2 that reaches the point O. Therefore, the two crests out of the two slits are in phase or superpose constructively at the point O. Suppose, on the other hand, the diffracted beam out of the slit 2 travels a length of l_1 and that of the slit 1 a length of l_2 such that the difference, $(l_2 - l_1)$, is one half the wavelength λ. Then the crest of the wave, for instance, out of the slit 1 arrives at the point P whereas the trough of the wave out of the slit 2 arrives there, the latter being out of phase by one half the wavelength. Therefore, their magnitudes cancel each other and they superpose destructively. In general, therefore, destructive superposition (node) occurs whenever the path difference Δl $(= l_2 - l_1)$ satisfies the following condition:

$$\Delta l = (j + \tfrac{1}{2})\lambda \qquad \text{for } j = 0, \pm 1, \pm 2, \pm 3, \ldots \tag{8.4a}$$

Constructive superposition (antinode) takes place when the following condition is satisfied:

$$\Delta l = j\lambda \tag{8.4b}$$

When the distance L between a barrier with slits and a screen is much larger than the slit separation d (refer to Fig. 8-6), the diffraction is called Fraunhofer diffraction; otherwise it is called Fresnel diffraction. In the case of Fraunhofer diffraction, the paths of lengths l_1 and l_2 are very nearly parallel so that the angles Ω_1

and Ω_2 are very nearly equal. Then one has with the angle Ω in Fig. 8-6:

$$\Delta l = d \sin \Omega \tag{8.5}$$

Further, cos Ω is nearly unity for very small Ω such that sin Ω = tan Ω ($= y/l$), leading to the following approximate relationship:

$$y = \frac{L(j + \frac{1}{2})\lambda}{d} \qquad \text{(minima or nodes)} \tag{8.6a}$$

and

$$y = \frac{Lj\lambda}{d} \qquad \text{(maxima or antinodes)} \tag{8.6b}$$

The same relationship holds (Jenkins and White, 1976) for multislit (N slits) diffraction for the maxima. An important difference, however, is that amplitude of the maxima is much greater for the multislit case. This is due to the fact that N waves are constructively superposed instead of only two. Also, the distance from a maximum to the next minimum is smaller than it is when there are two slits by the factor of $2/N$. The Fraunhofer diffraction patterns for two slits and six slits are shown in Fig. 8-7 for the same slit separation, screen distance, and wavelength for light of intensity I. The Fraunhofer diffraction limits the resolution of projection photolithography.

The Fresnel diffraction limits the resolution of proximity photolithography in which the mask is close to the wafer surface, as illustrated in Fig. 8-8. The

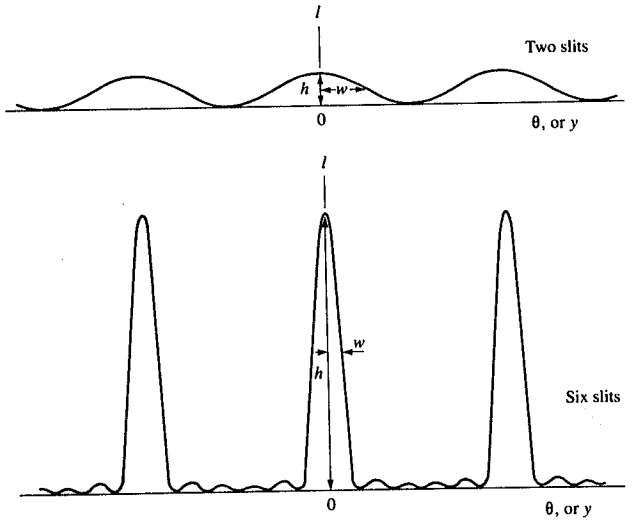

FIGURE 8-7
Diffraction patterns for two and six slits (Eisberg and Lerner, 1981).

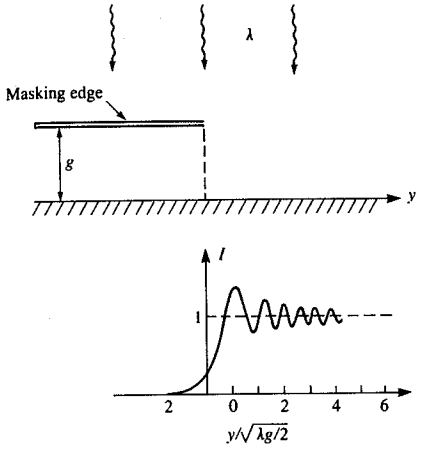

FIGURE 8-8
Fresnel diffraction at a masking edge (Trotel and Fay, 1980).

intensity of the beam on the wafer surface depends on the dimensionless variable, $y/(\lambda g/2)^{1/2}$ (e.g., Jenkins and White, 1976), if the focal length is taken as the gap g. Here λ is the coordinate shown in Fig. 8-8.

As with any electromagnetic wave, the intensity of a light wave is proportional to the square of its amplitude. The amplitude of the maxima of an N-slit diffraction pattern is proportional to N because of N combining waves that superpose in phase. Therefore, the intensity of the maxima is proportional to N^2. The fact that the distance from a maximum to the next minimum is proportional to $1/N$ together with the same maxima positions as indicated by Eq. (8.6b) for arbitrary N means that the width of the maxima is proportional to $1/N$. Although w in Fig. 8-7 is called simply the width, its full name is half-width at half-maximum intensity. A multislit device with a large value of N is called a diffraction grating and the spacing d between its slits is called the grating spacing. Combination of Eqs. (8.4) and (8.5) leads to the grating formula:

$$d \sin \Omega = j\lambda \tag{8.7a}$$

For the general case of a beam incident in arbitrary angle i, the grating formula (Jenkins and White, 1976) is

$$d(\sin i + \sin \Omega) = j\lambda \tag{8.7b}$$

where the integer j is known as the order.

Constructive and destructive superposition, or interference, also take place when a light beam passes through a medium and then is reflected at the interface adjoining the medium to another medium, e.g., at the interface between a resist and a substrate in photolithography. This interface also leads to standing waves as in diffraction, as shown in Fig. 8-9. It can be shown (Cuthbert, 1977) for perfect reflection at the interface (substrate surface in Fig. 8-9) that the antinodes

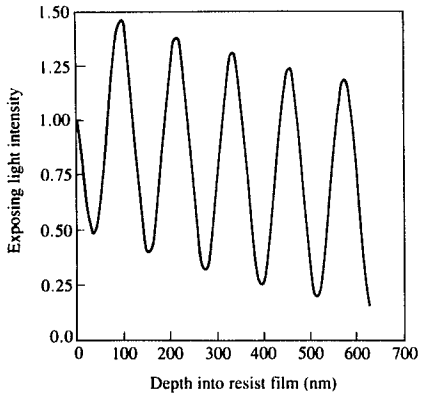

FIGURE 8-9
Light intensity distribution (standing wave) in a resist (Dill *et al.*, 1975a).

(maxima) and nodes (minima) are given by

$$n(l - z) = \begin{cases} \dfrac{(2j-1)\lambda}{4} & \text{(maxima)} \quad (8.8a) \\ \dfrac{j\lambda}{2} & \text{(minima)} \quad (8.8b) \end{cases} \qquad \text{for } j = 1, 2, 3, 4, \ldots$$

where l is the resist film thickness and z is the distance into the resist.

When the ratio of wavelength to slit width (λ/d) is very small, the diffraction effect is also very small and most of the light is not diffracted. In such cases, ray optics, as opposed to the wave optics considered so far, can be used. The basic law of ray optics is that light travels in straight rays, providing it travels through uniform material. This ray optics (also called geometric optics) is the basis for describing image formation by lenses. Central to the image formation is a quantity called focal length f shown in Fig. 8-10. All paraxial rays (rays that are near the centerline axis) emitted from a point on an "object" plane parallel to the plane of a converging lens will converge to a point on another parallel plane, the image plane, no matter where the point of emission is located. This occurs when the object distance, s, is greater than the focal length, f. The relationship between the object and image distances (s and s') and the focal length f in Fig. 8-10 is (e.g., Eisberg and Lerner, 1981)

$$\frac{1}{s} + \frac{1}{s'} = \frac{1}{f} \qquad (8.9)$$

Note that the magnification (h'/h in the figure) can be determined from s and s' using triangle similarity.

There are a number of quantities obtainable from the focal length and the lens aperture D. The numerical aperture (NA) often used in describing image formation is given by $D/2f$ and the F number is given by f/D. For the role of the numerical aperture, consider the refractive lens imaging system shown in Fig.

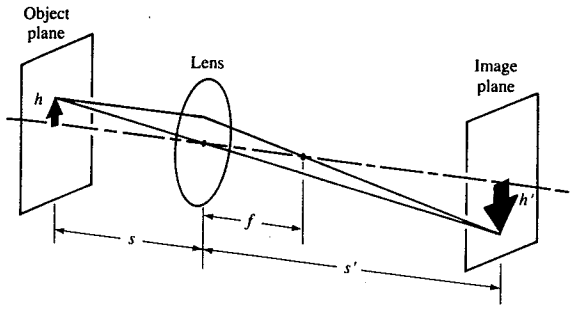

FIGURE 8-10
Image formation by a lens (Eisberg and Lerner, 1981).

8-11 (Thompson and Bowden, 1983). When light passes through a mask and has been diffracted, it is next imaged onto a wafer using an objective lens. The aperture in the figure is such that the objective lens can collect light from angles smaller than $2\alpha_o$, where α_o is the maximum cone angle of rays reaching the lens from the object point (mask). For a given magnification, the numerical aperture $(\text{NA})_o$ is related to α_o as follows:

$$(\text{NA})_o = n \sin \alpha_o$$

where n is the refractive index in image space and is usually equal to unity. Similarily, the numerical aperture of the condenser lens in Fig. 8-11 is given by

$$(\text{NA})_c = n \sin \alpha_c$$

Numerical aperture is thus a measure of the "acceptance" angle of a lens. It is important to recognize that images are formed by the intersection of rays of light

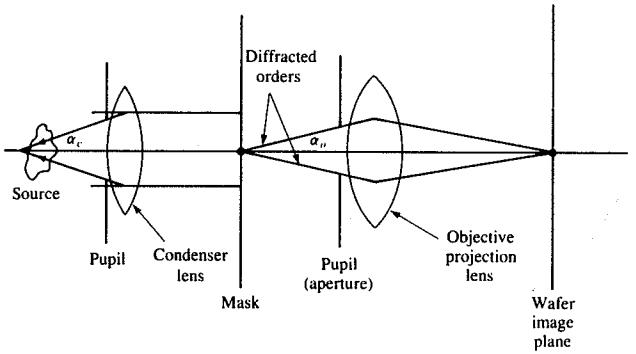

FIGURE 8-11
A refractive lens imaging system with partially coherent light (Thompson and Bowden, 1983).

which emanate from a point (Fig. 8-10) and that the pattern information is contained in the diffracted light (Fig. 8-11). The undiffracted or zero-order beam [$j = 0$ in Eq. (8.7*a*)] from an edge or grating constitutes only a single ray and at the very least a second ray emanating from the edge is needed to reconstruct an image of the edge. Therefore, the larger the numerical aperture of the projection lens is, the greater is the amount of diffracted information that can be collected and subsequently imaged.

A light beam is termed coherent when the angular range of light waves incident on the barrier with slits is small. Completely coherent illumination occurs when all beams pass through a slit in one angle. A beam is termed incoherent when the angular range of incident waves is large. Coherency is quantified in terms of the degree of coherency (Thompson and Bowden, 1983). It is defined in Fig. 8-12 for two common types of illumination where M is the magnification and the subscripts o, c, and s are for objective lens, condenser, and source, respectively. The degree of coherency is zero for a coherent source since it is a point

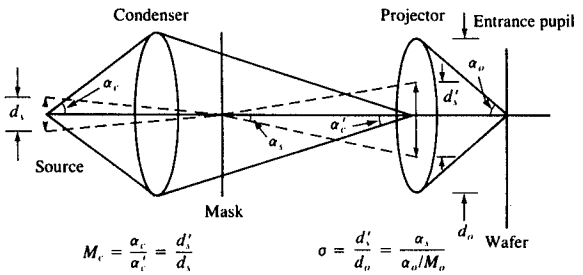

(*a*) Kohler

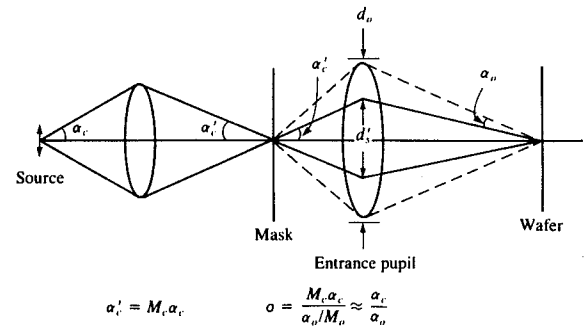

(*b*) Critical

FIGURE 8-12
Degree of coherency for two common types of illumination system (Thompson and Bowden, 1983).

source, i.e., zero diameter. The degree of coherency is infinite for an incoherent source. In reality, however, $\sigma \leq 1$ since all light collected from any real source is always imaged within the entrance pupil. In practice, partially coherent sources are used.

The basic laws governing light optics also apply to electron optics provided the square root of electrical potential is used in place of the index of refraction. The index of refraction is a measure of light velocity; the square root of the potential is a measure of electron velocity. In light optics, the brightness or luminous intensity is defined as the flux per unit solid angle emitted by a luminous source. By analogy the brightness B of a source of charged particles is defined as the current density J per unit solid angle Ω:

$$B = \frac{J}{\Omega} \tag{8.10}$$

If the current is emitted from (or converges toward) a small area through a cone of included half-angle α, the brightness can be approximated (Herriott and Brewer, 1980) by

$$B = \frac{J}{\pi\alpha^2} \tag{8.11}$$

if α (in radians) is small.

Electrons or a beam of electrons can be generated (extracted) from a crystalline material by giving sufficient energy to the conduction electrons such that they may overcome the potential well of the crystal lattice. Simple heating of a metal accomplishes this extraction and is called thermionic emission, the basic source of electrons for most practical vacuum electronic devices. Extraction can also be accomplished by applying an intense external electric field to the metal surface and this is termed field emission. When a beam of electrons is focused and directed to the surface of a resist material for imaging, the electrons entering the resist are scattered by interaction (collisions) with the atoms of the resist material. This scattering can be divided roughly into two classes: forward and backward scattering. Since most of the electrons (Greeneich, 1980) are forward scattered through small angles (less than 90°) from their original direction, this effect merely broadens the incident beam. Some electrons experience large-angle scattering (approaching 180°), causing these electrons to return to the surface. Electrons are scattered both elastically and inelastically. Elastic scattering results only in a change of direction of the electrons while inelastic collisions result in energy loss. Consequently, the incident electrons will spread out as they penetrate until all of their energy is lost or until they exit the solid as a result of backscattered deflections. The simulation of electron trajectories is very complex and a Monte Carlo method (Kyser and Viswanathan, 1975) is available for this purpose. The simulation results for 100 electrons are shown in Fig. 8-13. Note that most of the energy is absorbed in the silicon substrate.

For approximate results, it is sufficient to know the distance electrons penetrate and their radial distribution at any depth. An approximate maximum

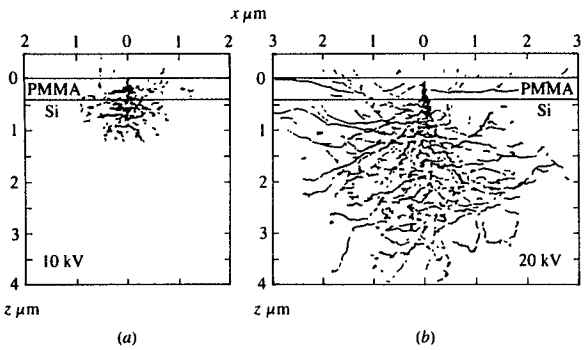

FIGURE 8-13
Monte Carlo simulated electron trajectories for 100 electrons scattered in a PMMA resist on a Si substrate (Kyser and Viswanathan, 1975).

penetration depth is known as the Grun range R_G, given (Everhart and Hoff, 1971) by

$$R_G\ (\text{cm}) = \frac{4.6 \times 10^{-6}}{\rho\ (\text{g/cm})} E_o^{1.75}\ (\text{keV}) \tag{8.12}$$

where E_o is the incident energy and ρ is the density. Based on the Grun range, Everhart and Hoff (1971) give the following for the average absorbed energy per volume E_v as a function of penetration depth z in the material:

$$E_v = \frac{DE_o}{qR_G}\lambda(f) \tag{8.13}$$

where

$$\lambda(f) = 0.74 + 4.7f - 8.9f^2 + 3.5f^3 \qquad \text{where } f = \frac{z}{R_G} \tag{8.14}$$

D is the incident charge per unit area, known as dose, and q is the electronic charge. The radial distribution at any depth for a point beam source can be approximated (Chang, 1975; Parikh and Kyser, 1978) by

$$E_v(r; z) = k(z)\left[\exp\left(-\frac{r^2}{\beta_f^2}\right) + \mu_e\left(\frac{\beta_f^2}{\beta_b^2}\right)\exp\left(-\frac{r^2}{\beta_b^2}\right)\right] \tag{8.15}$$

where β_f and β_b are the characteristic half-widths of the forward and backscattered distributions and

$$\mu_e = \frac{I_b}{I_f} \qquad \text{and} \qquad I_i = 2\pi\int_0^\infty r\exp\left(-\frac{r^2}{\beta_i^2}\right)dr \tag{8.16}$$

TABLE 8.1
Coefficients for the Gaussian approximation of Eq. (8.15) (Greeneich, 1980)

Substrate	Energy	Resist thickness	β_b or β_{bs}	β_{bd}	μ_e	μ_{ds}
Si	10	0.5	0.65	—	0.51	—
Si	15	0.5	1.14	—	0.51	—
Si	15	1.0	1.41	—	0.52	—
Si	25	0.5	2.6	—	0.51	—
Si	25	1.0	2.9	—	0.49	—
Si	25	1.5	2.9	—	0.52	—
Si	40	0.5	6.0	—	0.42	—
Si	40	1.0	6.0	—	0.45	—
Si	40	1.5	6.2	—	0.44	—
Cu	10	0.5	0.23	0.8	0.60	0.66
Cu	15	0.5	0.33	1.0	0.60	0.19
Cu	25	1.0	0.77	3.0	0.65	0.19
Cu	40	1.0	1.43	3.6	0.63	0.16
Au	10	0.5	0.16	0.5	0.65	0.9
Au	15	0.5	0.16	0.8	0.76	0.24
Au	25	1.0	0.37	1.4	0.79	0.28
Au	40	1.0	0.64	4.0	0.82	0.15

The backscattering effect given by the second term in Eq. (8.15) is mostly by the scattering from the substrate. In general, the parameters are determined from a Monte Carlo simulation (Hawryluk *et al.*, 1974) or experimental data. A relationship for β_f is shown in Fig. 8-12 where the number of elastic events P_e is given by

$$P_e = \frac{400z\ (\mu m)}{E_o\ (\text{keV})} \tag{8.17}$$

Values of the parameters β_b and μ_e are given in Table 8.1.

The dose-position function $\lambda(f)$ is relatively constant for small values of the normalized position f, goes through a maximum, and then decreases rapidly with f. The radial distribution of the energy dissipated is dominated by desired forward scattering, when the incident energy E_o is large, as should be evident from Eq. (8.17) and Fig. 8-14. Therefore increasing the incident energy (beam voltage) is desirable to a certain extent. There are, however, two limitations. The first is that the rate of energy dissipated per electron decreases as the beam energy is increased. Most of the energy is absorbed by the substrate when the energy is high (see Prob. 8.2). The second limiting aspect is the proximity effect discussed in Sec. 8.4. As the energy increases, there is more interaction between closely spaced features (proximity effect), limiting the resolution. In any event, a reduction in the resist thickness leads to a reduction in backscattering and thus to a smaller feature size. The resolution is usually defined in terms of the minimum feature that can be repeatedly exposed and developed in at least 1 μm of resist.

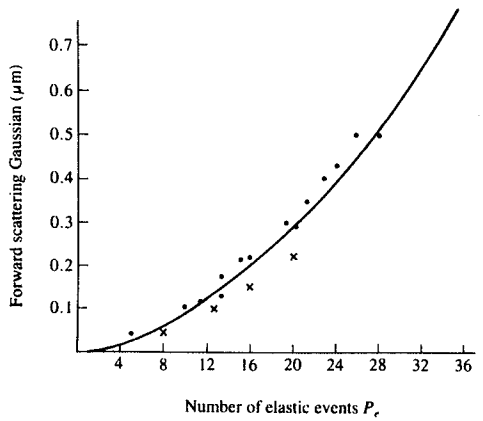

FIGURE 8-14
β_f as a function of number of elastic events (Greeneich, 1980).

Undesired scattering can be minimized if particles of higher mass than electrons are used. This has led to the use of ion beams. In fact, backscattering can be made almost absent with an ion beam for silicon substrates with a resist. Ionization by electron impact is the primary technique for generating ions. Electrons for ionization can be created by thermionic emission or can result from the discharge itself. These electrons are accelerated by the use of dc or rf fields and confined by the use of magnetic fields. An ion is generated when the energy transferred to a molecule by an accelerated electron exceeds the ionization energy for that molecule. Ions can also be generated by an electric field, termed field ionization.

As in electron-beam lithography, the quantities of interest in ion-beam lithography are the distance ions travel in a solid (resist and substrate) and the distribution of the energy imparted by the penetrating ions. The two main mechanisms of energy transfer are nuclear collisions and electronic interactions (Brodie and Muray, 1982). The energy loss by nuclear collisions results from collisions between nuclear charges and the target atoms. The second energy loss mechanism involves the interaction of the fast ion with the lattice electrons. An approximate ion range R_i resulting from the two energy loss mechanisms (Brodie and Muray, 1982) is

$$R_i = 2kE_o\left(1 - \frac{4kk'E_o}{3}\right) \tag{8.18}$$

where E_o is the incident energy and k and k' are given (Schwartz and Helms, 1979) by

$$k\ (\text{Å/eV}) = \left(\frac{0.018}{N}\right)\left[\frac{(Z_1^{2/3} + Z_2^{2/3})^{1/2}}{Z_1 Z_2}\right]\left(\frac{M_1 + M_2}{M_1}\right) \tag{8.19}$$

$$k'\ (\text{Å}^{-1}) = 0.328(Z_1 + Z_2)M_1^{-1/2} \tag{8.20}$$

Here Z and M are the atomic number and the mass, the subscripts 1 and 2, respectively, are for the ion and lattice atoms, and N is the atomic density (particles/Å^3). The first term in Eq. (8.18) represents the nuclear collisions and the second the electronic interactions. Since the backscattering can be neglected, the radial energy distribution can be represented only by the first term in Eq. (8.15). Here, again, Monte Carlo simulations (Karapiperis *et al.*, 1981) similar to the electron-beam calculations can be used.

The resolution-limiting diffraction effects in photolithography can be reduced by switching from the usual ultraviolet (300 to 400 μm) to deep-ultraviolet light whose wavelength is half as large, or almost eliminated by using soft x-rays whose wavelengths are several orders of magnitude smaller. This can be seen from Eqs. (8.3) and (8.4). If the wavelength λ is very small, Δl in the equations that define the maxima and minima is so small that there is almost no distinction between the nodes and antinodes and the interference effects become negligible. Soft x-rays, those with wavelengths between 0.1 and 5 μm, behave differently from lower energy photons in that they are neither significantly reflected nor refracted by any material. Therefore, they are not suitable for projection lithography. For this reason, the only currently feasible form of x-ray lithography is shadow lithography in which the pattern, formed of regions opaque and transparent to x-rays, is transferred to a nearby resist layer, as shown in Fig. 8-15.

The soft x-rays suffer negligible scattering as they pass through materials. They essentially move in straight lines until captured by an atom with ejection of a photoelectron (Wittels, 1980). The material is most transparent to x-rays when their wavelength is slightly longer than a "critical wavelength" and most opaque when it is shorter. The x-ray beam flux (energy per area per time) I decreases exponentially with penetration depth z:

$$I = I_0 \exp(-\mu z) \tag{8.21}$$

where μ is an absorption coefficient. The energy dissipated in a resist layer is proportional to the energy removed from the beam:

$$E_v(z) = \mu I(z) = \mu I_0 \exp(-\mu z) \tag{8.22}$$

The absorption coefficient, which is dependent on wavelength, is given in Fig. 8-16 for various materials (Spiller and Feder, 1977).

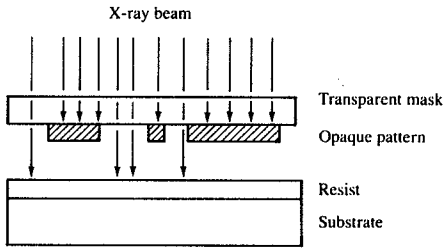

FIGURE 8-15
X-ray shadow lithography (Wittels, 1980).

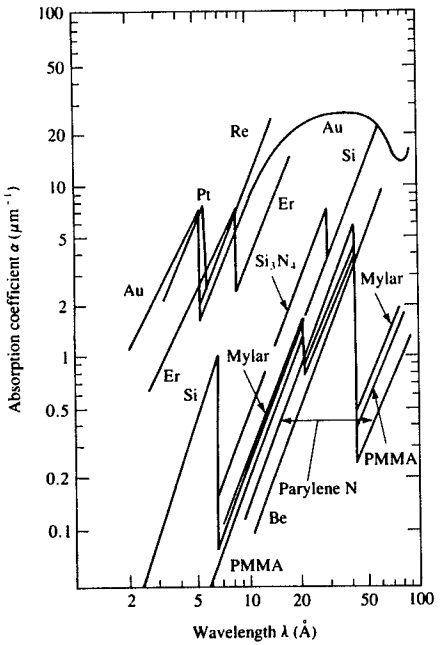

FIGURE 8-16
Absorption coefficients for x-rays as a function of wavelength (Wittels, 1980).

8.3 ILLUMINATION AND PATTERN TRANSFER

The first step in mask and device fabrication is to expose a resist (or an emulsion in the case of the photographical method) to a beam of monochromatic light, x-ray, electrons, or ions so that the pattern image can be transferred to the resist, which contains a component sensitive to the beam. The resolution and delineation of the pattern to be transferred depends on the beam intensity, its spatial distribution and the beam width.

The methods of pattern transfer (imaging) vary with the beam source. Contact, proximity, or projection printing can be used for light beams. Because of the poor contrast with soft x-rays, shadow printing is used, which is a form of proximity printing, as shown in Fig. 8-15. The three different methods used for the optical lithography are illustrated in Fig. 8-17 along with the corresponding typical optical intensity pattern (Skinner, 1973). The oldest method is contact printing (imaging) in which the mask and the resist are in direct contact. The major drawback on the contact method is poor yield. Defects in the mask can be caused by small particles on the wafer surface, which leave scratches, etc. These altered mask sites are copied along with the original pattern on subsequent wafers. However, very high resolution up to 0.5 μm is possible. Other photolithographic techniques can approach but not exceed its resolution capabilities. The defect problem can be avoided by providing a gap (10 to 25 μm) between the mask and resist, which is the essence of the proximity printing. The resolution is proportional to $(\lambda g)^{1/2}$, where λ is the monochromatic light wavelength and g is the gap (McGillis and Fehrs, 1975) and is on the order of a few micrometers. Projection printing involves projecting an image of the pattern onto the resist surface. Since the mask is far away from the resist-coated wafer, only a small portion of the mask is imaged at a time to achieve high resolution. This small image field necessitates scanning or stepping over the surface of the wafer and therefore the method is also called step-and-repeat printing. Resolution can be made close to that possible with contact printing.

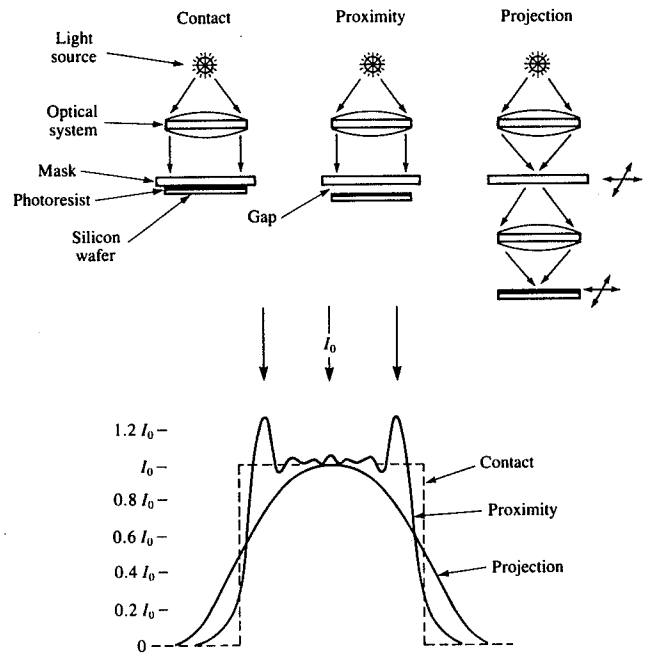

FIGURE 8-17
Schematics of three methods of optical lithography and the corresponding intensity patterns (McGillis, 1983).

Although masks are used for printing in general, maskless printing is also used. In maskless printing the image is generated on a resist directly without a mask. A typical example is mask fabrication with e-beams. Maskless printing should become a major method in time for wafer processing in spite of the slow speed with which a wafer can be processed. This is the major impediment to the

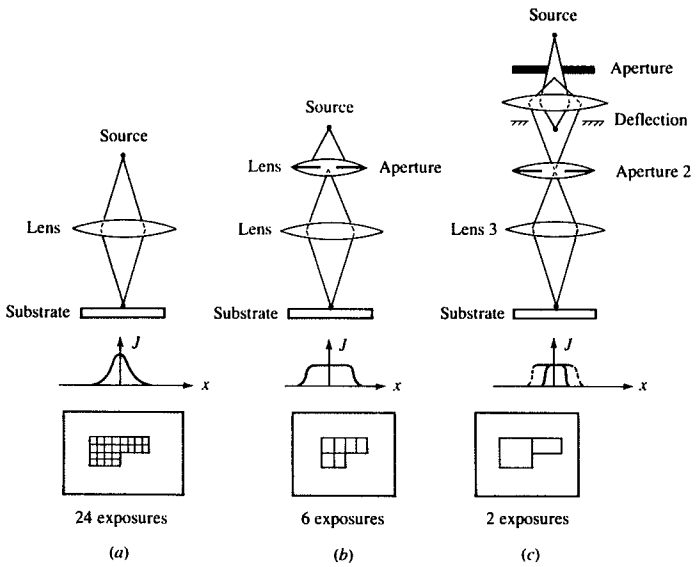

FIGURE 8-18
Spot-forming strategies in scanning e-beam lithography (Wittels, 1980).

maskless particle-beam lithography. In maskless printing a beam is focused to a spot the same size as or smaller than the minimum pattern size. With the combination of beam deflection and shuttering, individual spot exposures are built up into complete patterns that are stored on a tape in accordance with the digitized circuit layout. Different spot-forming strategies are used in scanning particle-beam lithography. These are shown in Fig. 8-18 (Wittels, 1980). In the simplest system (Fig. 8-18*a*), the source is imaged directly on the substrate, and the beam current density distribution is Gaussian. A spot size a small fraction of the minimum feature size is necessary for good pattern fidelity and, as seen in the figure, 24 exposures are necessary for the example. In the shaped beam case (Fig. 8-18*b*), the spot size is made equal to the minimum feature size. The Gaussian edge of the current density profile results only from lens aberrations and not the source characteristics. In a variable-shaped beam (Fig. 8-18*c*), the image of the first illumination-filled aperture is deflected by the intermediate deflection unit and then imaged onto the second aperture. Thus, variable shapes can be imaged on the wafer. The current density edge profile remains the same as that of the spot size.

Now let us consider photolithography in some detail. The limiting factor in the lateral dimension of a single pattern in photolithography is diffraction: Fresnel diffraction in the case of proximity printing and contact printing, and

Fraunhofer diffraction in the case of projection printing. The resolution depends on how much tolerance can be allowed in the intensity and the line width. According to Lin (1980), it is

$$\frac{W^2}{\lambda Z} \geq 0.5 \qquad \text{for proximity printing} \tag{8.23}$$

$$W \geq \frac{0.6\lambda}{\text{NA}} \tag{8.24a}$$

for projection printing

$$Z \leq \frac{0.8\lambda}{(\text{NA})^2} \tag{8.24b}$$

where W is the resolution and Z is a limit on the depth of focus over which image quality is not degraded. If the resist thickness is larger than Z, given by Eq. (8.24*b*), the latent image cannot be focused throughout the resist depth. The first relationship corresponds to the dimensionless distance in Fig. 8-8 that yields an intensity of approximately unity. For a coherent beam, $0.5\lambda/(\text{NA})$ corresponds to the half-width of the principal diffraction peak and $0.5\lambda/(\text{NA})^2$ is the defocusing aberration for the principal peak (also known as the depth of focus). The numbers in Eqs. (8.24) reflect the effect of partial coherence on the allowed tolerances.

When a beam of constant intensity is shined on a mask, the intensity is the same as the incident beam for contact printing, as shown in Fig. 8-17. Because of edge effects due to Fresnel diffraction in proximity printing (see Fig. 8-8), the intensity distribution on the wafer is that shown in Fig. 8-17 for a single slit.

An approach based on a transfer function called the modulation transfer function (MTF) is used in projection printing to relate the incident intensity (input) to the spatial distribution of the intensity of the image on a wafer (output) (see Prob. 8.17). This is similar to the transfer functions often used in the field of process control. Instead of the time frequency used in process control, the MTF uses a spatial frequency, defined as the number of slits or line pairs (each consisting of a slit opening and the spacing in between) per unit length. MTF is a measure of the accuracy of image transfer with respect to sharpness or contrast. Consider a model 1:1 projection printing, shown in Fig. 8-19 (Thompson and Bowden, 1983). The mask consists of a grid of periodic opaque lines and transparent spaces of equal widths. The diffraction of light at the edge of an opaque feature results in the projected pattern or image in the photoresist exhibiting gradual (rather than sharp) transitions from light to dark. Therefore, the edges of the projected feature appear blurred rather than sharp because of considerable light in the middle of the opaque feature. MTF of an exposure system is defined as the ratio of the modulation in the image plane to that in the object plane. The modulation M is defined in Fig. 8-19. For a given spatial frequency, the contrast of the projected image is greater for higher MTF values (see Prob. 8.17 for MTF calculations for a sinusoidal object, which is used to approximate a square wave object).

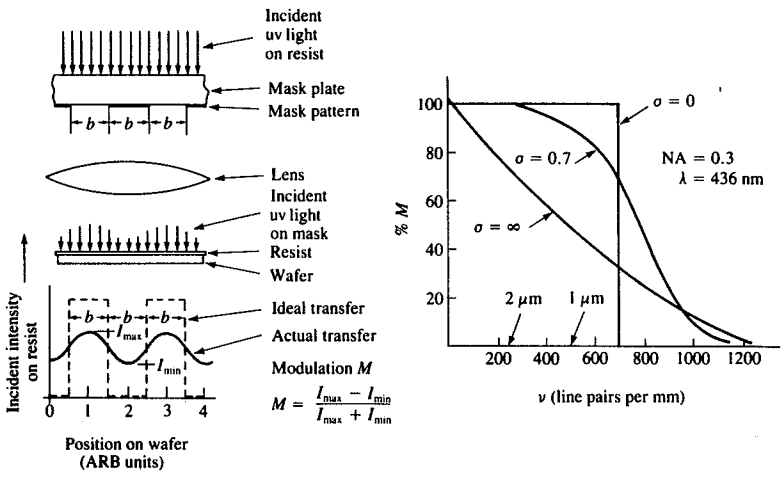

FIGURE 8-19
(*a*) Schematic of image transfer efficiency for a 1:1 projection (Bowden, 1981) and (*b*) MTF (%*M*) as a function of spacial frequency for three coherency factors (Thompson and Bowden, 1983).

The primary parameter in the MTF is the critical spatial frequency f_c (see Prob. 8.17) that defines the maximum number of slits allowable for imaging. The general grating formula of Eq. (8.7*b*) for primary diffraction ($j = 1$) can be rewritten as

$$\frac{\sin i + \sin \Omega}{\lambda} = \frac{1}{d} = f \tag{8.25}$$

where d (length of a pair of lines consisting of the slit opening and the spacing between slits) is $2b$ in Fig. 8-19. For image formation, it is required that $i, \Omega < \alpha$, where α is the angle that a focused ray makes with the screen (wafer). The maximum f or f_c is that corresponding to the case of $i = \Omega = \alpha$, and since $\sin \alpha$ in air is (NA), one has [from Eq. (8.25)]

$$f_c = \frac{2(\text{NA})}{\lambda} \tag{8.26}$$

This critical spatial frequency is the maximum number of repeating slits, each consisting of the slit opening plus the spacing between slits that can be contained per unit width without losing the image. At f_c, the MTF is zero. For most organic photoresists, the MTF has to be larger than 0.4 for good imaging. The MTF is very sensitive to spatial frequencies near the critical spatial frequency for a coherent beam but not for incoherent or partially incoherent beams as shown in Fig. 8-19*b*. Note that $\sigma = 0$ for a coherent beam and $\sigma = \infty$ for an incoherent beam. This is the major reason that a partially coherent beam is used in projection printing. A partially coherent source with a value of σ around 0.7 yields optimum pattern reproduction in conventional photoresists (Thompson and Bowden, 1983).

Example 8.1. Photolithography uses an ultraviolet (uv) beam with wavelength around 400 nm. Suppose that deep uv projection lithography uses a beam of 200 nm. For the beams of 200 and 330 nm, calculate the depth of focus, the minimum feature size that can be obtained, and the maximum possible number of lines that can be printed per unit width. Discuss the effect of the wavelength on the projection performance. Assume the numerical aperture (NA) to be 0.17.

Solution. From Eq. (8.24*a*), the minimum feature sizes are

$$W_{200} \geq \frac{0.6 \times 200 \text{ (nm)}}{0.17} = 707 \text{ nm} = 0.706 \ \mu\text{m}$$

$$W_{330} \geq \frac{0.6 \times 330}{0.17} = 1165 \text{ nm} = 1.165 \ \mu\text{m}$$

From Eq. (8.24*b*), the depths of focus are

$$Z_{200} \leq \frac{0.8 \times 200 \text{ (nm)}}{(0.17)^2} = 5.54 \ \mu\text{m}$$

$$Z_{330} \leq \frac{0.8 \times 330}{(0.17)^2} = 9.14 \ \mu\text{m}$$

The respective maximum possible spatial frequencies, or number of lines per unit width, follows from Eq. (8.26):

$$(f_c)_{200} = \frac{2(\text{NA})}{\lambda} = \frac{2 \times 0.17}{200 \text{ (nm)}} = 1.7 \text{ lines/}\mu\text{m} = 1700 \text{ lines/mm}$$

$$(f_c)_{330} = \frac{2 \times 0.17}{330} = 1030 \text{ lines/mm}$$

The following brief table summarizes these results:

λ, nm	W, μm	Z, μm	f, lines/mm
200	0.7	5.5	1700
330	1.2	9.1	1030

It is seen that as the wavelength decreases, the minimum feature size decreases with a corresponding increase in the number of lines that can be written per unit width. However, the resist thickness to which the feature can be imaged (Z) decreases with

decreasing wavelength. Thus, for the 200-nm beam, the resist should not be thicker than 5.5 μm whereas it could be as thick as 9.1 μm for the 330-nm beam.

In scanning e-beam lithography, the current density of the Gaussian beam is given by

$$J = J_p \exp\left[-\left(\frac{r}{\beta}\right)^2\right] \tag{8.27}$$

where β is the standard deviation of the distribution and J_p is the source current density. The total current I in this beam is given by $I = \pi\beta^2 J_p$. For some purposes the actual Gaussian beam is treated as an equivalent beam of uniform current density, J_p, with a Gaussian beam diameter, d_G (Herriott and Brewer, 1980) such that the current is expressed as $I = \pi J_p d_G^2/4$, which means that $d_G = 2\beta$. The actual beam diameter d_G is given by

$$d_G = \frac{1}{\alpha}\left(\frac{I}{3.08B}\right)^{1/2} \tag{8.28}$$

where B is the brightness given by Eq. (8.11).

8.4 RESISTS

Resists are of a polymeric material that serves as a medium by which the device pattern can be imprinted onto the wafer or mask surface. As such, the resist is one of the main factors determining the resolution and delineation of the transferred pattern. Depending on the sensitizing (radiating) source, resists are termed photoresists, x-ray resists, e-beam resists, and so on. The same resist can sometimes be used for different sensitizing sources.

Although resists for wet processing are of interest here, there are also resists for dry processing in which the resists are etched away for desired patterns by colliding ions as in plasma etching (Chap. 10). Resists can also be classified into inorganic and organic resists. Inorganic resists have been used only recently (Yoshikawa *et al.*, 1976). An example is a thin layer of Ag_2Se on top of a film of Ge_xSe_{1-x} glass (Tai *et al.*, 1982). The species sensitive to light is Ag. Migration of Ag into the underlying glass upon exposure to light leads to the desired pattern.

Organic resists consist of either only one component or two components. Two-component resists are made from an inert resin that serves only as a binder and film-forming material. They contain in the resin a sensitizer molecule which in general is monomeric in nature and undergoes the chemical transformations that are responsible for imaging. Photoresists are invariably two-component resists. One-component resists are polymers that have radiation sensitivity. They are a single, homogeneous material. Most e-beam resists are one-component resists.

In the common negative resists, the exposure to radiation yields an insoluble, crosslinked polymer. In the process of dissolving the unexposed polymer to obtain the final pattern, the crosslinked position swells and often distorts. For this reason, positive resists are usually preferred when feature sizes are in the submicrometer range.

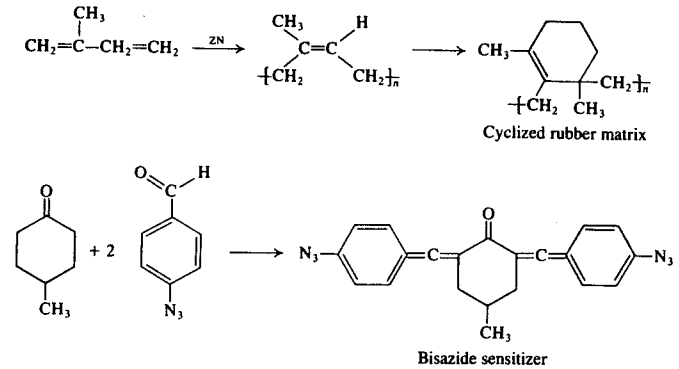

FIGURE 8-20
Formation of poly(*cis*-isoprene) and bisazide photosensitive compound.

The classical two-component negative photoresist is a cyclized polyisoprene synthetic rubber matrix with bisarylazide photoactive compound such as Kodak's KTFR. The poly(*cis*-isoprene) is produced by Zeigler-Natto polymerization of isoprene followed by proprietary treatments which cyclize the polymer. The photoactive compound is produced by a condensation reaction combining *para*-azido benzaldehyde with a substituted cyclohexanone as in Fig. 8-20.

The response of the sensitizer to incident light is generation of a crosslinked, three-dimensional network. The azide group emits a nitrogen molecule to form a highly reactive nitrene intermediate. The nitrene may combine with another nitrene to form an azo dye, enter a carbon-hydrogen bond to form an amine, remove a hydrogen atom from the polymer backbone to form an amine radical and a carbon radical, or enter the double bond of the polymer to form an aziridene linkage as in Fig. 8-21.

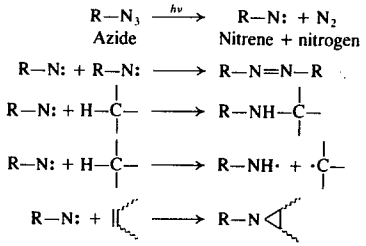

FIGURE 8-21
Crosslinking reactions of bisazide sensitizer and poly(*cis*-isoprene).

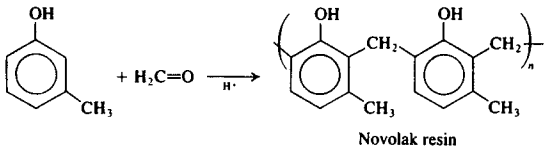

FIGURE 8-22
Novolac polymer formation.

The positive two-component photoresists are replacing the negative photoresists in many applications because of their higher resolution and better resistance to dry etching. The matrix portion of the positive resist is a novolac resin, while a diazoquinone is used for the photoactive compound. Novolac resin is a copolymer of a phenol and a formaldehyde, as shown in Fig. 8-22. The phenolic group of the novolac matrix imparts an acidic character which enables the resin to be dissolved in an aqueous base (Willson, 1983). The phenolic reactants used for production of novolac are a mixture of *meta*-cresol (60%), *para*-cresol (30%), xylenols, and *ortho*-cresol. The *meta*-cresol is much more reactive and generates a high molecular weight, very crosslinked polymer if it is the only phenolic monomer, while pure *para*-cresol produces a low molecular weight polymer that is unusable as a resist matrix. Variations in viscosity and developer solubility require extensive blending of production lots to produce a consistent product (Pamplone, 1984).

The diazonaphthoquinone sensitizer acts to inhibit solubility of the resist in aqueous base until it is exposed to light. Upon exposure, an excited state is produced which evolves nitrogen to form a carbene intermediate. The carbene then

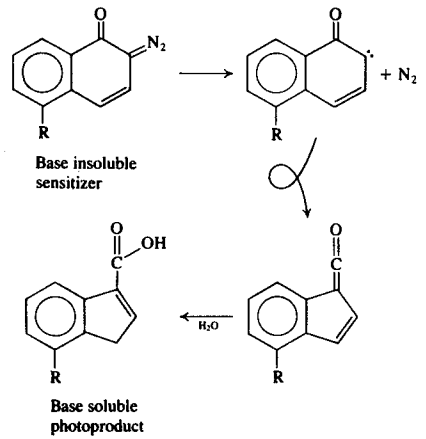

FIGURE 8-23
Transformation of diazonaphthoquinone photoactive compound to carboxylic acid. R is usually an aryl sulfonate.

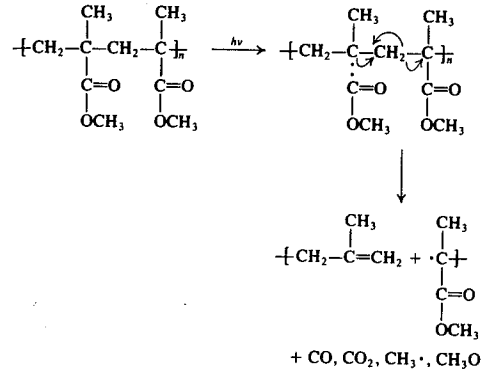

FIGURE 8-24
Mechanism of PMMA chain scission initiated by carbonyl–main chain carbon homolysis.

undergoes a Wolff rearrangement to produce a ketene. The ketene intermediate then adds water present in the resist film to produce an indenecarboxylic acid product that is soluble in the aqueous base developer (Willson, 1983) (Fig. 8-23).

The classical electron-beam resist is poly(methyl methacrylate), PMMA, a positive one-component resist. PMMA is produced from the methyl methacrylate monomer by a radical initiated polymerization catalyzed by azo-bis-isobutyronitrile. It has extremely high resolution but its relatively low sensitivity, 50 to 100 $\mu C/cm^2$ at 20 keV exposure, and poor resistance to plasma and reactive ion etching limit its usefulness (Willson, 1983).

The initial effect of radiation upon PMMA resist is homolysis of the bond between the main chain and carbonyl carbons to form a stable radical on the main chain (see Fig. 8-24). The chain is cleaved by beta scission rearrangement of the radical, resulting in an acyl-stabilized radical. The process may also be initiated by homolysis of the carbonyl carbon-oxygen sigma bond. Decarbonylation follows, resulting in the same tertiary radical. Wet development with an organic solvent that dissolves only the low molecular weight material resulting from chain scission is used to produce the image. The poly(olefin sulfones) are alternating copolymers of sulfur dioxide and an alkene. Despite the drawback of thermal instability, high sensitivity and low materials cost have attracted and maintained interest in these polymers.

Exposure of poly(olefin sulfones) to radiation causes scission of the carbon-sulfur bond followed by cationic and radical depolymerization to produce the olefin and sulfur dioxide monomers (see Fig. 8-25). Minor products include alkanes corresponding to loss of the side chain group and removal of the side chain radical by the olefin monomer (Bowmer and O'Donnell, 1982).

The most widely used negative electron-beam resist is COP, a copolymer of glycidylmethacrylate and ethyl acrylate. COP is produced by a radical copolymerization in benzene solvent with a benzoyl peroxide initiator.

The epoxy group in the glycidyl side chain of COP is the portion of the molecule that responds to radiation. Upon exposure, a cation, cationic radical,

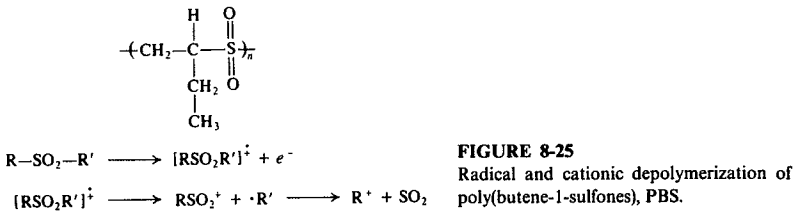

FIGURE 8-25
Radical and cationic depolymerization of poly(butene-1-sulfones), PBS.

anion, or anionic radical is formed which initiates a crosslinking chain reaction (see Fig. 8-26). The epoxy group is opened to generate the crosslinking bond and another reactive oxygen species. This chain reaction mechanism makes COP a relatively sensitive material but also causes a "dark reaction" which may continue after exposure (Willson, 1983). More details on resists can be found in Willson (1983).

The demands placed upon a potential resist material are great. Since the lithographic process is repeated in its entirety several times for each wafer, the sensitivity of the resist is a primary concern. Another major issue is contrast, as it has been shown that the contrast value and the resolution of a resist are directly related. Ideally, the limit of the feature size that can be produced will be dictated by the writing and etching procedures, not the exposure characteristics of the resist. Also, the resist must have adequate film-forming properties when spin-coated, such as adhesion to the substrate, and resistance to acid, base and reactive ion etching. The response of the resist to small, daily variations in process

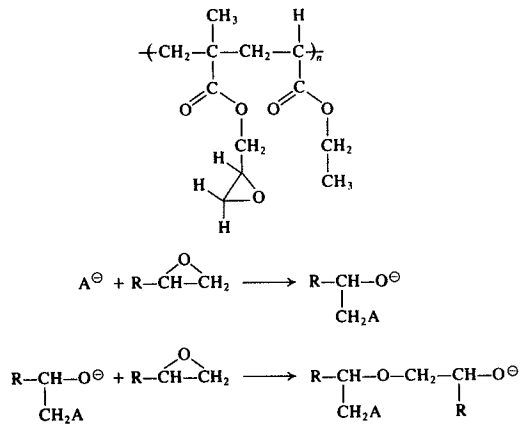

FIGURE 8-26
Glycidyl methacrylate-co-ethyl acrylate, COP. Anionic crosslinking mechanism.

conditions should be minimal, and a shelf-life of three or more months is considered adequate (Thompson and Bowden, 1983).

8.5 RESIST DEVELOPMENT

Depending on the types of resists, the exposed parts, when dissolved (developed) in a solvent, become either more readily soluble (positive resists) or less soluble (negative resists) than the unexposed parts. The reason for the difference in the dissolution rate is the change in the average molecular weight of polymer due to the exposure for e-beam resists. For photoresists, on the other hand, the reason is the transformation of the inhibitor that inhibits dissolution into a species soluble in a solvent. However, some photoresists dissolve by the same mechanism as for e-beam resists. The resists whose dissolution behavior owes their characteristics to changes in molecular weight (mostly e-beam resists) will be considered first.

There are two types of transformation that occur when the resists are exposed to radiation. Depending on the radiation-sensitive group in the resist, the polymer either goes through crosslinking resulting in a higher molecular weight polymer or decomposes through bond-breaking (scission) to a lower molecular weight polymer. The solubility of a polymer in a solvent, in general, decreases with increasing molecular weight. Therefore, the exposed part of the resist dissolves when the irradiation results in a decrease in the molecular weight. When the irradiation leads to an increase in the molecular weight, the exposed part remains intact while the unexposed part dissolves. The chemical transformation taking place upon irradiation requires a certain activation energy. Therefore, the amount of the polymer going through the transformation is determined by the amount of energy it receives and whether the energy source is photon (light), x-ray, electron, or ion. This in turn means that the energy (or radiation intensity) distribution, considered in Sec. 8.2, determines the shape of the resist when it is developed in a solvent.

The molecular weight distribution resulting from the irradiation varies with the position in the resist. The local, number-averaged molecular weight M for positive resists can be expressed (Herzog *et al.*, 1972; Greeneich, 1975) as

$$M = \frac{M_0}{1 + \mu(E_v)} \tag{8.29}$$

where M_0 is the initial number average molecular weight. The average number of scissions per molecule, μ, is a function of the absorbed energy per unit volume, E_v, and is given by

$$\mu = \frac{GE_v M_0}{mN_A} \tag{8.30}$$

where m is the mass density of the polymer, N_A is Avogadro's number, and G is the number of chain scissions per unit dissipated energy and is dependent only on

the chemical nature of the polymer. Equation (8.29) is a simple mass balance, since the number of chain scissions per molecule, μ, generates $(1 + \mu)$ fragments (decomposed parts) of total weight M_0 and new average molecular weight M. For the case of a negative resist, G in Eq. (8.30) can be defined as the net number of average crosslinkings directly responsible for the molecular weight increase, since crosslinking and scission can take place simultaneously. Then one has, for the negative resist (see Prob. 8.14),

$$M = (1 + \mu)M_0 \tag{8.31}$$

For a given resist, the development (solubility) rate, usually expressed in length per time, is dependent on the type of solvent and its concentration. In much the same way as in the gas-solid reactions (Chap. 5), the development (penetration) front can be diffused or sharp (shell-progressive) depending on the relative rate of dissolution with respect to the rate of the penetration (diffusion) of the solvent. An ideal situation is one in which the development front moves in a shell-progressive manner with time. For a given resist, the solvent and its concentration can be chosen for the purpose (Ouano, 1984).

The development rate for positive polymeric resists is often correlated in a power-law form. The correlation of Greeneich (1975) is rewritten in the following form so that it can be applicable to both positive and negative resists:

$$R = R_0 + k_d\left[\left(\frac{M_0}{M}\right)^{\alpha} - 1\right] \tag{8.32}$$

where k_d is a rate constant in the form of an Arrhenius relationship and α is the order in a kinetic reaction sense. R_0 is the solubility rate of the resist in the absence of irradiation. In general, it is small for positive resists but large for negative resists. If a solvent and its concentration are chosen in such a way that the resist is almost impermeable to the solvent, the dissolution is limited to the surface being dissolved and the observed rate is that at the rate dictated by the intrinsic kinetics of dissolution. Under the conditions, the progression of the dissolution can be written (see Prob. 8.15) as follows:

$$\frac{dz}{dt} = R(z, x) \tag{8.33}$$

where x is the direction perpendicular to the resist depth coordinate z.

The concepts of contrast and sensitivity are used in evaluating a resist and the key parameter is energy dose, defined as photons or electrons per unit area. The dose is equal to the photon or electron intensity multiplied by the exposure time t_r and the typical units are coulombs per square centimeter for electrons and calories (ergs) per square centimeter for photons. The contrast Ω is defined as

$$\Omega = \left|\log\left(\frac{D_f}{D_i}\right)\right|^{-1} \tag{8.34}$$

where D_f is the extrapolated dose for full thickness, as shown in Fig. 8-27 for

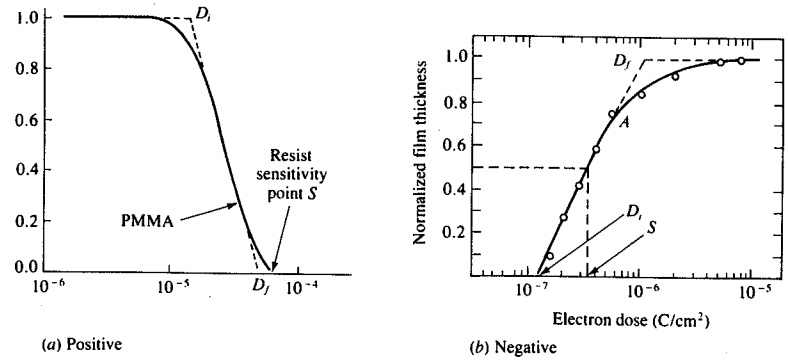

(*a*) Positive (*b*) Negative

FIGURE 8-27
Determination of contrast for positive and negative resist (Greeneich, 1980).

both negative and positive resists, and D_i is the idealized minimum dose necessary for the dissolution. The contrast is a measure of the slope of the line representing the resist thickness remaining after development (normalized with respect to the final resist thickness) as a function of dose. The contrast is directly related to the resolution capability of a resist. The higher the contrast is, the better are the resolution and the edge definition of a resist.

The sensitivity S is the minimum dose that gives dimensional equality of clear and opaque features. For the negative resist in Fig. 8-27, this is taken as the dose at which the remaining resist thickness is 50 percent. For positive resists, all of the resist material must be removed to be useful and hence the sensitivity is that at the complete removal point, as shown in Fig. 8-27. Although the contrast, as defined by Eq. (8.34), has mostly been used in electron- and ion-beam lithography, the same definition can be used for photoresists. Noting that μ in Eqs. (8.29) and (8.31) is much larger than unity and that μ is proportional to the absorbed energy E_v, for a given resist, it follows from these equations that M_0/M is proportional to E_v for positive resists and is inversely proportional to E_v for negative resists. Since the dose D is proportional to the energy, it follows from Eq. (8.32) that the development rate due to the irradiation, which is $R - R_0 + k_d$, is proportional to D^{α} for positive resists and $D^{-\alpha}$ for negative resists. The contrast is given by the logarithm of the slope of the line for the fraction of resist dissolved plotted against the dose. Therefore, the order α is a measure of the contrast, the value being higher for higher contrast.

The definition of sensitivity, which can be determined experimentally, allows one to find a minimum feature size that can be obtained in an e-beam resist. For the satisfactory development of the resist, it has to receive a certain number of electrons per unit area for the necessary chemical transformation of polymers in the resist. If the minimum dimension for a line is denoted by l_p, the

minimum number of electrons required (N_{min}) for the sensitivity S is

$$N_{min} = \frac{Sl_p^2}{q} \tag{8.35}$$

The area corresponding to l_p^2 is called a picture element or pixel. The minimum dimension, therefore, follows from Eq. (8.35):

$$l_p = \left(\frac{qN_{min}}{S}\right)^{1/2} \tag{8.36}$$

An important conclusion that can be drawn from Eq. (8.36) is that the minimum dimension is inversely proportional to the square root of the sensitivity. Since electron emission is a random process, a question arises as to the probability of the number of electrons that will strike a given surface. The limit imposed by a probabilistic argument is 200 for N_{min} (Greeneich, 1980). Then Eq. (8.36) yields

$$l_p = \left(\frac{200q}{S}\right)^{1/2} \tag{8.37}$$

where N_{min} is taken as 200.

Example 8.2. Poly(methyl methacrylate), or PMMA, is a positive resist. Greeneich (1975) correlated his extensive data on the development rate R as follows:

$$R = A + \frac{B}{M^{\alpha}} \tag{A}$$

For PMMA, he arrived at the following set of parameters for two types of solvents:

Developer† (solvent)	T, °C	A, nm/min	B	α
MIBK:IPA (1:3)	22.8	0	9.33×10^{13}	3.86
MIBK:IPA (1:3)	32.8	0	1.046×10^{15}	3.86
MIBK	22.8	8.4	3.154×10^{7}	1.50
MIBK	22.8	24.2	5.67×10^{7}	1.50

† MIBK = methyl isobutyl ketene, IPA = isopropyl alcohol.

Calculate the development rates at 22.8 and 32.8 °C for the mixed solvent (MIBK + IPA) at the uniform molecular weight, M, of 3.4×10^3. Calculate the development time for 310 nm PMMA resist.

Solution. According to Eq. (A),

$$R_{22.8} = \frac{9.33 \times 10^{13}}{(3.4 \times 10^3)^{3.86}} = 2.18 \text{ nm/min}$$

$$R_{32.8} = 24.44 \text{ nm/min}$$

Therefore the development rate depends strongly on temperature. Since the rate is uniform everywhere, Eq. (8.33) for the dissolution rate can be integrated with $z = 0$ at $t = 0$ to give

$$z = Rt \quad \text{or} \quad Z = Rt_f \tag{B}$$

For Z of 310 nm, one has, from Eq. (B),

$$t_f = \frac{310}{R}$$

Thus,

$$(t_f)_{22.8} = \frac{310}{2.18} = 142.2 \text{ min}$$

$$(t_f)_{32.8} = \frac{310}{24.44} = 12.68 \text{ min}$$

The strong dependence of the development time on temperature should be noted.

Example 8.3. Consider the PMMA in Example 8.2 (310 nm thick) coated onto a silicon substrate. An electron beam of 1 μm diameter of constant intensity is used such that the dose is 5×10^{-5} coulomb/cm^2. For the following data, calculate the development time at 22.8 °C with the mixed solvent. [Note that the energy density (and thus the molecular weight) varies with the depth. Assume the radial energy density to be uniform.]

$$E_o = 20 \text{ keV} \qquad \rho = 1.2 \text{ g/cm}^3$$

$$G = 19 \text{ keV}^{-1} \qquad M_0 = 2 \times 10^5$$

Solution. From Eq. (8.12),

$$R_G = \frac{4.6 \times 10^{-6}}{\rho \text{ (g/cm}^3\text{)}} E_o^{1.75} \text{ (keV)} = \frac{4.6 \times 10^{-6} \times 20^{1.75}}{1.2} = 7.25 \ \mu\text{m} \tag{A}$$

The axial energy density is given by Eq. (8.13):

$$E_v = \frac{DE_o}{qR_G} \lambda(f)$$

$$= \frac{5 \times 10^{-5}}{1.6 \times 10^{-19}} \times \frac{20}{7.25 \times 10^{-4}} \lambda(f)$$

$$= 8.62 \times 10^{18} \text{ (keV/cm}^3\text{)} \lambda(f) \tag{B}$$

The axial molecular weight distribution is given by Eq. (8.29):

$$\frac{M}{M_0} = \frac{1}{1+\mu} \tag{C}$$

where $$\mu = \frac{GE_v M_0}{mN_A} = \frac{19 \times 8.62 \times 10^{18}\lambda(f) \times 2 \times 10^5}{1.2 \times 6.02 \times 10^{23}}$$

$$= 44\lambda(f)$$

Since $\mu \gg 1$, one can rewrite Eq. (C) as

$$M = \frac{mN_A}{GE_v}$$

$$= \frac{1.2 \times 6.02 \times 10^{23}}{19 \times 8.62 \times 10^{18}\lambda(f)} = \frac{4411}{\lambda(f)} \qquad \text{(D)}$$

From Eq. (8.33) and Eq. (A) in Example 8.2,

$$\frac{dz}{dt} = \frac{9.33 \times 10^{13}}{M^{3.86}} = 9.33 \times 10^{13}\left(\frac{\lambda}{4411}\right)^{3.86} \quad \text{(nm/min)} \qquad \text{(E)}$$

where Eq. (D) has been used. In terms of f, $z = R_G f$. Thus, Eq. (E) can be rewritten as

$$\frac{df}{dt} = \frac{0.798}{R_G}\lambda^{3.86} = \frac{0.798}{7250}\lambda^{3.86}$$

$$= 1.10 \times 10^{-4}(0.74 + 4.7f - 8.9f^2 + 3.5f^3)^{3.86} \qquad \text{(F)}$$

The time required follows from Eq. (F):

$$t_f = \int_0^{0.0428} \frac{df}{1.10 \times 10^{-4}(0.74 + 4.7f - 8.9f^2 + 3.5f^3)^{3.86}} \qquad \text{(G)}$$

since the resist thickness normalized with respect to R_G is 0.0428. Numerical integration of Eq. (G) based on three points, for illustration, yields t_f of 815 minutes. If the uniform molecular weight assumed in Example 8.2 were 6139, which corresponds to the M value at the surface in this example, the required time would be 122 minutes at 22.8 °C for Example 8.2.

The edge shape of the dissolved resist in the above example is perfectly straight since the radial (lateral) energy density distribution was assumed to be uniform. In reality, however, the edge is not perfectly straight because of electron scattering. This is shown in Fig. 8-28 for three different doses (Hatzakis, 1975). The first is typical of the case of high doses, relative to the resist thickness. If the dose is high enough, scattering, which widens the opening toward the resist-substrate interface, is also sufficiently high to cause substantial scission of polymer even in the region dominated by backscattering. Thus, the region readily dissolves when developed, causing widening toward the interface. In the other extreme of low doses, not much scission occurs and the dissolution is mainly dependent on how long the resist is developed. Therefore, the shape in the bottom of Fig. 8-28 results. Note in this case that the resist thickness is considerably reduced due to prolonged development, compared to the other cases. A combination of the two extreme cases, in which both the energy dissipation distribution and development time contribute, leads to the straight shape shown in the middle of Fig. 8-28. The shape of the developed resist can be simulated based on the Gaussian profile given by Eq. (8.15) (see Prob. 8.2).

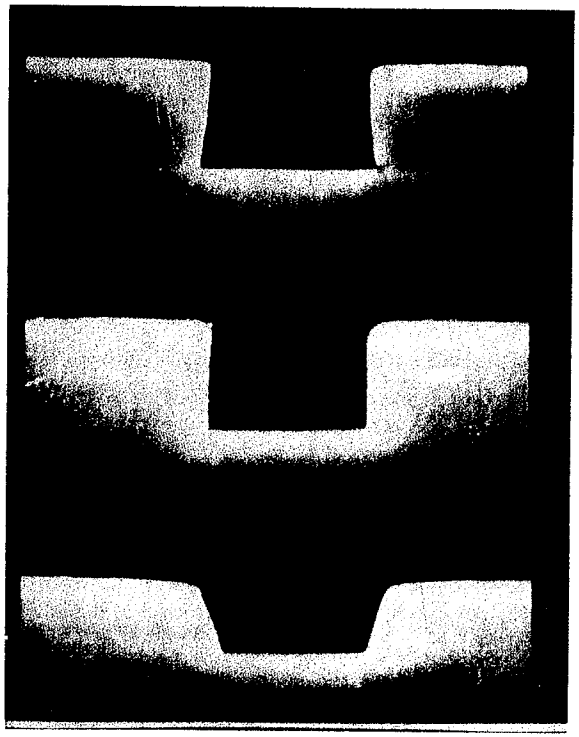

FIGURE 8-28
Actual cross-sectional views of PMMA resist profiles at high (undercut), intermediate (vertical), and low (undercut) doses (Hatzakis, 1975).

Similar procedures, as used for the electron beam, can be followed for the development of a resist exposed to an ion beam. R_G in Eqs. (8.12) and (8.13) is replaced by R_i given by Eq. (8.18), and the penetration range function (depth-dose function), $\lambda(f)$, similar to Eq. (8.14) must be known. Because of negligible backscattering, only the first term in Eq. (8.15) for the forward scattering can be used for the lateral energy distribution.

Another major effect of the scattering of particle beams is called the proximity effect. Scattering leads to the overlapping of patterns in close proximity to one another. The proximity effect is strongly dependent on the electron energy since high-energy exposures have large exposure tails and these tails, when overlapped, lead to the effect. Procedures for correcting the proximity effect hinge on this recognition. Dose manipulations are used for the purpose (Parikh, 1980).

Unlike the electron-beam resist, a positive photoresist contains an inhibitor component that prevents dissolution in a solvent. The inhibitor readily absorbs photons and then goes through a chemical transformation upon exposure, leading to the disappearance of the inhibitor, and the resist becomes soluble in a suitable solvent. The typical solvents are dilute aqueous alkaline solutions. The negative photoresist, however, behaves much the same as the electron-beam resist in that the absorption of photons leads to crosslinking of polymers.

Because of the nature of the inhibitor, the concentration distribution of the inhibitor largely determines the development process. The rate of inhibitor concentration normalized with respect to the initial inhibitor concentration, M, is often assumed (Dill *et al.*, 1975a) to be dependent on the light flux I_m and to be of first order with respect to the concentration:

$$\frac{\partial M}{\partial t} = -k_i I_m M \tag{8.38}$$

where k_i is a pseudo rate constant. As the light passes through the resist, the intensity decreases and this change follows the Beer-Lambert law (Chap. 5):

$$\frac{\partial I_m}{\partial z} = -\alpha I_m \tag{8.39}$$

where α is the absorption constant and z is the resist depth coordinate. Since the inhibitor absorbs photons, the absorption constant is proportional to the inhibitor concentration:

$$\alpha = AM + B \tag{8.40}$$

where A and B are constants that are dependent on photoresist type. The rate of development is in turn dependent on the inhibitor concentration M. A correlation proposed by Dill *et al.* (1975b) is

$$R \text{ (nm/s)} = \exp (a_1 + a_2 M + a_3 M^2) \tag{8.41}$$

where a_1, a_2, and a_3 are constants. More physically based models are given by Kim *et al.* (1984) and Hershel and Mack (1987).

Example 8.4. For a positive photoresist that is 0.545 μm thick on a silicon substrate, Dill *et al.* (1975b) gave the following parameters:

$$A = 0.54\ \mu\text{m}^{-1} \qquad B = 0.03\ \mu\text{m}^{-1} \qquad k_i = 0.014\ \text{cm}^2/\text{mJ}$$

The incident beam intensity I_0 was 57 mJ/(cm^2·s) for the wavelength of 436 nm and the constants for the development rate are

$$a_1 = 5.96 \qquad a_2 = -1.19 \qquad a_3 = -2.27$$

Assuming that the incident beam intensity is uniform laterally and 1 μm wide, calculate a minimum exposure time required for the inhibitor concentration at the resist-substrate interface to be less than 1 percent. The minimum time may be defined as the time corresponding to M of unity throughout the resist for the purpose of calculating $I_m(z)$. Describe a numerical method of calculating the required, actual exposure time for the 1 percent inhibitor concentration at the interface. Note that, at time zero,

$$M(z, 0) = 1$$

$$I_m(z, 0) = I_0 \exp [-(A + B)z]$$

and at $z = 0$,

$$I_m(0, t) = I_0$$

$$M(0, t) = \exp (-k_i I_0 t)$$

Solution. Combination of Eqs. (8.39) and (8.40) yields

$$\frac{\partial I_m(z, t)}{\partial z} = -[AM(z, t) + B]I_m$$

$$= -(0.54M + 0.03)I_m \tag{A}$$

Equation (8.38) is

$$\frac{\partial M(z, t)}{\partial t} = -0.014 M I_m \tag{B}$$

For the minimum exposure time, M is unity throughout the resist for the purpose of calculating the intensity. Equation (A) integrated with $M = 1$ is

$$I_m(z) = I_0 \exp (-0.57z) \tag{C}$$

Use of Eq. (C) in (B) and integration of the resulting equation yields

$$M(z, t) = \exp \left[-\int_0^t 0.0141 I_0 \exp (-0.57z)\, dt \right]$$

$$= \exp [-0.798t \exp (-0.57z)] \tag{D}$$

At the interface ($z = 0.584$ μm), M is 0.01. Thus, from Eq. (C),

$$0.01 = \exp [-0.572t]$$

The minimum time, therefore, is 8.05 s.

The maximum time for the required condition of 1 percent M at the interface is that corresponding to $M = 0$ in Eq. (A), or $I(z) = I_0 \exp (-0.03)$. Use of this in Eq. (D) yields

$$M(z, t) = \exp [-0.798t \exp (-0.03z)]$$

$$= \exp (-0.014t)$$

Thus, the maximum time is 329 s. The actual time is between 8 s and 329 s.

For the actual time, Eqs. (A) and (B) are written in the following Euler form:

$$I_l(i+1, j) = -[0.54M(i, j) = 0.03]I_m(i, j)\,\Delta z + I_m(i, j) \qquad i = 0, 1, 2, \ldots \qquad \text{(E)}$$

$$M(i, j+1) = -0.014M(i, j)I_m(i, j)\,\Delta t + M(i, j) \qquad j = 0, 1, 2, \ldots \qquad \text{(F)}$$

Since the starting points $[M(i, 0), M(0, j); I_m(i, 0), I_m(0, j)]$ are known, a computer program based on Eqs. (E) and (F) should yield the actual time. The subscripts i and j, respectively, are the grid points for z and t. Equation (E) is first used to calculate the axial I_m profile at time zero ($j = 0$). Based on the profile, time is incremented by Δt and the axial M profile is calculated for the incremented time, which is then used in Eq. (E) for the corresponding I profile. These procedures can be repeated until the time at which M at the interface becomes 0.01. This time is the required exposure time.

Example 8.5. For the same problem in Example 8.4, calculate the time required for the development of the resist. Assume that the final inhibitor concentration profile at the end of the exposure is given by

$$M(z) = z$$

Solution. For the parameters given in Example 8.4, Eq. (8.41) is

$$R = \exp(5.96 - 1.19M - 2.27M^2) \quad \text{(nm/s)}$$

$$= 10^{-3} \exp(5.96 - 1.19M - 2.27M^2) \quad (\mu\text{m/s}) \qquad \text{(A)}$$

Use of the M profile in Eq. (A) yields

$$R\ (\mu\text{m/s}) = 10^{-3} \exp(5.96 - 1.19z - 2.27z^2) \qquad \text{(B)}$$

From Eq. (8.33),

$$\frac{dz}{dt} = R(z)$$

or

$$t_f = \int_0^{0.584} \frac{dz}{R(z)} \qquad \text{(C)}$$

Integration of the right-hand side of Eq. (C) based on an equidistant (seven-points) use of the trapezoidal rule yields

$$t_f = 3.07 \text{ s}$$

The development time reported by Dill *et al.* (1975b) is an order of magnitude larger, indicating that the exposure time was very short and that the actual $M(z)$ was much larger than that used in the example.

Although the incident beam imaged on the photoresist is uniform laterally in its intensity for contact printing and, to a certain extent, even for proximity printing, the intensity distribution is not uniform in the case of projection printing, as shown in Fig. 8-17. As illustrated in Prob. 8.17, this intensity distribution can be determined through the MTF. The intensity distribution caused by light diffraction is the reason why the width of the rectangular opening in Fig. 8-29 is

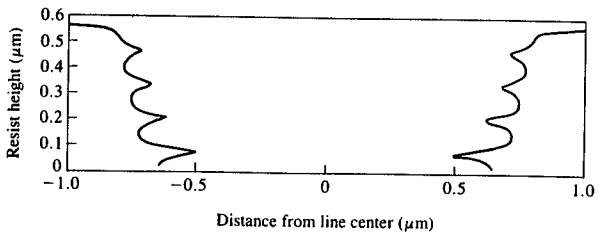

FIGURE 8-29
Positive photoresist edge profile after development (Dill *et al.*, 1975b).

larger toward the top. When light travels in a resist, it also reflects, and this reflection causes a standing wave within the resist (refer to Fig. 8-9) in much the same way as diffraction causes a standing wave (Cuthbert, 1977). The effect of this standing wave results in the wavy-edge shape shown in Fig. 8-29, which is a simulation result (Dill *et al.*, 1975b).

Example 8.6. The lateral intensity distribution of the incident light beam imaged on the resist surface by projection printing can be well approximated by a Gaussian distribution (see Prob. 8.12):

$$I_m = I_i \exp(-a_0 x^2) \qquad \text{(A)}$$

where a_0 is a constant. Write a sufficient set of equations necessary to simulate the development profile for the incident beam.

Solution. For a given exposure time, one has

$$\frac{\partial M}{\partial t} = -k_i M(z, x, t)I_m(z, x, t) \qquad \text{(B)}$$

$$\frac{\partial I_m}{\partial z} = -[AM(z, x, t) + B]I_m(z, x, t) \qquad \text{(C)}$$

Equations (A), (B), and (C) need to be solved numerically to obtain the inhibitor concentration distribution $M(z, x)$ at the end of the exposure. With the distribution, Eq. (8.33) can be used to determine the development profile along with a development rate such as Eq. (8.41).

Example 8.7. The contrast given by Eq. (8.34) is a measure of the slope of the resist thickness still remaining after development (F) with respect to the dose (D), and as such it can be rewritten as

$$\Omega = \frac{\partial F}{\partial \ln D} \qquad \text{(A)}$$

For the data given in Fig. 8-27 for a negative resist, determine the contrast line, i.e., a relationship between F and $\ln D$ for the straight line. Determine the exposure time

corresponding to D_f and that for the actual full thickness. Assume for 10 keV that the current flux is 10^{-8} A/(cm^2·s). Note that $D_i = 1.2 \times 10^{-7}$ and $D_f = 10^{-6}$ coulomb(C)/cm^2.

Solution. Integrating Eq. (A),

$$F = 0.472 \ln D + b \tag{B}$$

The dose is given by

$$D = Jt \tag{C}$$

where J is the current flux. For $D = D_f = 10^{-6}$,

$$t = \frac{D}{J} = \frac{10^{-6}}{10^{-8}} = 100 \text{ s}$$

The actual dose for the full resist thickness in Fig. 8-27 is 5×10^{-6} C/cm^2. Thus, the corresponding time is

$$t = \frac{D}{J} = \frac{5 \times 10^{-6}}{10^{-8}} = 500 \text{ s}$$

Postexposure bake and low-temperature prebake (softbake) of resists can enhance the imaging and development characteristics (Batchelder and Piatt, 1983). In the case of positive resists, more residual water in the resist following softbake can eliminate potentially uncontrollable crosslinking. Elimination of standing waves is also possible with a proper bake.

8.6 EDGE SHAPE AND ALIGNMENT

The edge shapes of the resist after development are dominated by diffraction effects in photolithography and by scattering in electron beam lithography. A straight edge is the ideal shape in almost all cases. The edge shape, as determined by electron scattering and resist development, has been discussed in the previous section. As shown in Fig. 8-18, the pattern and the corresponding line width can be obtained by a combination of single beam spots, each of which is of Gaussian distribution in its intensity or energy. The spot diameter of the beam is given by Eq. (8.28) and can be as small as 0.05 μm, in the practical energy range, i.e., sufficient energy for polymer scission or crosslinking for the development. Although the edge shape can be controlled with proper dose and development it is of interest to know how the edge shape changes with the beam half-width. The characteristic parameters are the Gaussian beam half-width, β_g, and the half-width of forward scattering, β_f. A correlation based on an effective half-width, β_e, which is given by $(\beta_f^2 + \beta_g^2)^{1/2}$, is shown (Greeneich, 1980) in Fig. 8-30. The relative edge slope at the resist-substrate interface would be infinite for the ideal, straight edge. It is seen from the figure that a relatively higher slope results for a smaller β_e. The Gaussian half-width can be reduced by properly placing or scanning several single beams side by side with the edges overlapping so that the relatively flat center region becomes large. In fact, this is a typical practice in scanning e-beam lithography. According to Eq. (8.17) and Fig. 8-14, a smaller β_f results when the resist thickness is small and the incident energy is large. Because of the sensitivity of the linewidth to backscattering that dominates the scattering effects at high energy, the increase in the incident energy for a smaller β_f should be limited to the range in which forward scattering dominates. For negative electron resists, the resist thickness distribution after development by exposure to a single scanning Gaussian beam of radius r_0 is given (Heidenreich *et al.*, 1975) by

$$p = 0.434\Omega\left(1 + \ln\left\{\exp\left(-\frac{x^2}{r_0^2}\right) + \exp\left[-\left(\frac{2r_0 - x}{r_0}\right)^2\right]\right\}\right) \tag{8.42}$$

where p is the thickness normalized with respect to the initial resist thickness. The edge shape follows from this relationship.

In photolithography, the edge shape is dictated by Fresnel diffraction in proximity printing. The energy distribution and the corresponding shape of the developed resist have already been discussed.

Example 8.8. For negative resists, the value of the contrast usually lies between 0.6 and 1. For a Gaussian e-beam of 0.5 μm diameter and a resist of 0.9 contrast,

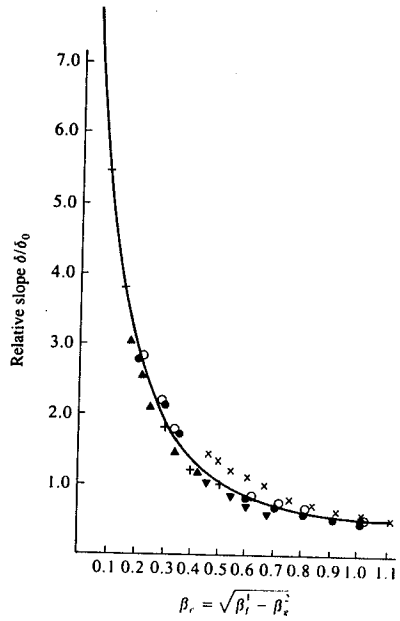

FIGURE 8-30
Relative edge shape as determined by effective beam half-width (Greeneich, 1980).

calculate the edge length, i.e., the lateral length of the resist still remaining after development that is in excess of the beam diameter. The experimental value (Heidenreich *et al.*, 1975) is approximately 0.46 μm.

Solution. The length in excess of the beam diameter can be obtained by finding the point x at which the resist thickness is zero, that is, $p = 0$ in Eq. (8.42). Thus, one has, from Eq. (8.42),

$$0 = 0.43\Omega\left(1 + \ln\left\{\exp\left(-\frac{x^2}{0.25^2}\right) + \exp\left[-\frac{(1-x)^2}{0.25^2}\right]\right\}\right)$$

or

$$-1 = \ln\left\{\exp\left(-\frac{x^2}{0.0625}\right) + \exp\left[-\frac{(1-x)^2}{0.0625}\right]\right\}$$

A value of 0.74 for x satisfies the equation, which means that the excess length l_e is given by

$$l_e = 0.74 - 0.25 = 0.49\ \mu\text{m}$$

As discussed in the previous section, the straight-edge shape is accomplished by properly manipulating both the dose level and the development time. In projection printing photolithography, the light beam is reflected by mirrors for the edge control so that it arrives at an angle rather than perpendicularly to the resist surface. This leads to the energy profile in the resist that is wider at the resist-substrate interface than at the resist surface. Proper manipulation of development time then yields straight edges.

Each time a masking level is added for further processing, the new mask features have to be properly aligned to the pattern already in the resist from the previous masking level so that the device can be fabricated according to the composite layout. The same is true with maskless processing using particle beams. Another factor to consider is the level of tolerance that must be allowed for uncertainties in mask alignment and deviations of the resist image from the mask image. This tolerance is one of the design rules used to lay out the circuit. An estimate of the nesting tolerance can be made if the distributions of developed resist feature sizes and registration are known. Registration is a measure of how closely successive mask levels can be overlaid. If the standard deviation in the developed resist-feature size for mask level 1 is β_1 and that for the level 2 is β_2 with the registration standard deviation of β_r, the tolerance T is given by

$$T = 3\left[\left(\frac{\beta_1}{2}\right)^2 + \left(\frac{\beta_2}{2}\right)^2 + \beta_r^2\right] \tag{8.43}$$

where the distributions are assumed to be normal. For this tolerance, the probability that the edge of a developed (etched) feature from level 1 will touch a feature from masking level 2 is approximately only 0.1 percent (McGillis, 1983).

Although an optical microscope can be used to align a mask to the wafer pattern with the aid of alignment marks on the wafer, the accuracy is only of the order of 0.25 to 0.5 μm. For better accuracy and automation, however, laser

interferometric alignment (e.g., Bouwhuis and Wittekock for photolithography, 1979; Alles *et al.*, 1975) and chip-by-chip e-beam alignment techniques are used.

8.7 OTHER CONSIDERATIONS, YIELD, AND ULTIMATE LIMITS

The fact that a thinner resist leads to a higher resolution has led to a technique of using multilayered resists. There are oxide or metal steps on a device that are 1 μm or so high. The first layer of the resist is applied to cover the previously patterned device topography on a silicon wafer. This leads to a planar surface. A very thin resist imaging layer is then spun on top of the planarizing layer. Only the top layer is used as a resist and the other layers are removed using the top resist as a mask. Another version of multilevel resists involve exposing and developing all resist layers. The resist layers are not necessarily of the same material (Saotome *et al.*, 1985). A form of multilayer structure was originally developed for the metal lift-off process (Havas, 1976). Multilayer structures are also used for patterning by reactive ion etching. In this case, the thin layer is used as a mask and the underlying thick layer then serves as an etch mask against reactive ion etching for subsequent pattern transfer into the underlying substrate (Moran and Maydan, 1979).

Defects in lithography are imperfections in a pattern. Some defects are fatal in that they lead to an inoperative device; others are cosmetic in nature. Types of defects commonly encountered on a process line are shown in Fig. 8-31. For the lithography based on masks, defects that are large enough to be resolved by the lithographic process will be transferred to the wafer and cause defects in devices.

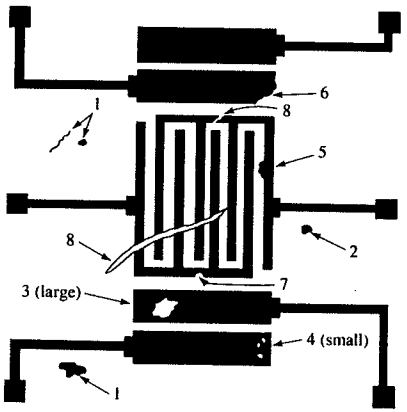

1 Contamination
2 Opaque spot
3 Large hole
4 Pin hole
5 Excess material
6 Lack of adhesion
7 Intrusion
8 Scratch

FIGURE 8-31
Types of defects (Ballantyne, 1980).

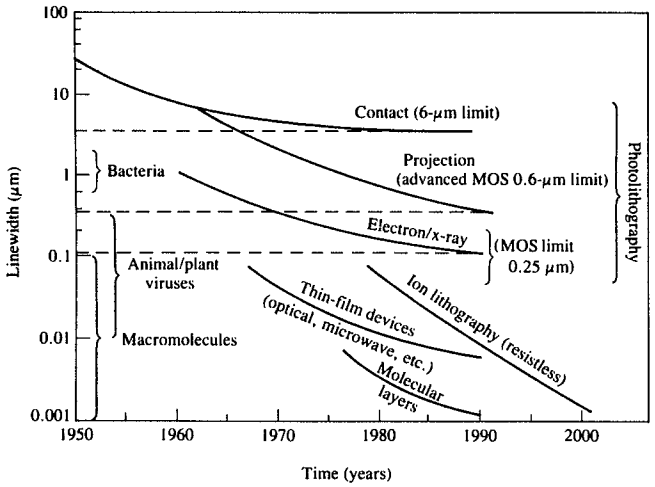

FIGURE 8-32
Linewidth of microelectronic devices and lithographies as a function of time (Brodie and Muray, 1982).

Further, each lithographic step generates additional defects which will combine to reduce the total process yield of good devices. A relationship (Price, 1970) between potential device yield Y and defect density (defects/area) is

$$Y = \prod_{i=1}^{n} (1 + X_i)^{-1} \tag{8.44}$$

where $X_i = D_i A_w$. The average defect density on the ith mask level is D_i, A_w is the wafer area, and n is the number of mask levels.

If it is assumed that X_i is the same for all levels, that is, $X = X_i$, Eq. (8.44) becomes

$$Y = (1 + X)^{-n} \tag{8.45}$$

One can see how rapidly chip yield decreases as the number of mask levels (n) increases. At $X = 0.3$, for instance, the yield decreases from 0.27 to 0.07 as the number of mask levels increases from 5 to 10 according to Eq. (8.45). The usual number of mask levels ranges from 7 to 10.

As the device size continues to decrease and the technology advances, the minimum feature size is going to be ultimately limited (Brodie and Muray, 1982) by the uncertainties dictated by the uncertainty principle of Heisenberg:

$$\Delta l \, \Delta p \geq \frac{h}{4\pi} \tag{8.46}$$

where Δl (μm) is the uncertainty (errors) in the coordinate of a particle, Δp is the uncertainty in its momentum, and h is Planck's constant. For photons, Eq. (8.47) can be rewritten as

$$\Delta l \ (\mu\text{m}) \geq \frac{hC}{4\pi E} = \frac{1.23}{E \ (\text{eV})} \tag{8.47}$$

Likewise, one can write similar equations for electrons and ions:

$$\Delta l \ (\mu\text{m}) = \begin{cases} \dfrac{h}{(2mE)^{1/2} 4\pi} = \dfrac{1.22 \times 10^{-3}}{[E \ (\text{eV})]^{1/2}} & \text{(electrons)} \quad (8.48) \\ \dfrac{h}{(2mE)4\pi} = \dfrac{2.74 \times 10^{-5}}{[(M/M_p)E]^{1/2}} & \text{(ions)} \quad (8.49) \end{cases}$$

where C is the speed of light, E is the beam energy, m is the electron mass, M is the ion mass, and M_p is the mass of the proton. This position uncertainty limits the sharpness of the line edge. For photon beams in the visible range this line edge uncertainty is in the 0.5 μm range; for electron beams it is about 1 Å for $E = 10^3$ eV. However, it is on the order of 10 nm if one includes the low-energy electron contribution and the proximity effect (Wallmark, 1979). It appears that the ultimate limit on the linewidth is in the range of 20 nm. The limiting values on the linewidth and the corresponding technologies (Brodie and Muray, 1982) are shown in Fig. 8-32. In the physical limits of the 10 to 20 nm range indicated in the figure, one would encounter fundamental questions on the device physics and on the traditional planar approach that are now accepted and practiced.

NOTATION

a_1, a_2, a_3	Constants in Eq. (8.41)
A, B	Constants in Example 8.2; constants in Eq. (8.40)
A_w	Wafer area
B	Brightness given in Eq. (8.10)
C	Concentration of resist solution (percent solid); light speed in vacuum
d	Distance from the top of a slit to that of an adjacent slit
d_G	Gaussian beam equivalent diameter given by Eq. (8.28)
D	Dose (C/L^2), incident charge per unit area; lens aperture; defects per area
D_f	Extrapolated dose for full thickness in Fig. 8-18
D_i	Minimum dose necessary for polymer dissolution
E_o	Incident energy (E)
E_T	Threshold energy
E_v	Energy per volume
f	Z/R_G; focal length defined in Eq. (8.9) and Fig. 8-10; spatial frequency (L^{-1})
f_c	Critical spatial frequency given by Eq. (8.26)
g	Gap between mask and resist (L)

G	Number of chain scissions or crosslinking per dissipated energy (E^{-1})
h	Planck's constant
I	Current; intensity (E/t)
I_b, I_f	Quantities defined in Eq. (8.16)
I_l	Light energy flux
j	Integer
J	Current flux (A/L^2t), often referred to as current density
J_p	Maximum J in Eq. (8.10)
$k(z)$	Normalizing factor dependent on resist depth in Eq. (8.15)
k, k'	Constants given by Eqs. (8.19) and (8.20), respectively
k_d	Rate constant in Eq. (8.32)
k_0	Constant in Eq. (8.43)
K	Constant in Eq. (8.1)
l	Resist thickness; distance a light travels for imaging
l_e	Edge length
l_p	Minimum dimension for a line in Eq. (8.36)
Δl	Difference between two light beams
L	Distance between barrier with slits and screen
m	Mass density; edge slope in Eq. (8.43)
M	Molecular weight of polymer; normalized inhibitor concentration in Eq. (8.38)
M_0	Initial value of M
M_1, M_2	Mass of ion and lattice atoms, respectively
MTF	Modulation transfer function (see Prob. 8.17 for tabulated values)
n	Refractive index defined by Eq. (8.1)
N	Number of slits; atomic density (atoms/L^3)
N_A	Avogadro's number
$N_{\min}$	Minimum number of electrons for the sensitivity S
NA	Numerical aperture ($D/2f$)
p	Normalized resist thickness
P	Total pressure
P_e	Number of elastic events given in Fig. 8-12
q	Electronic charge
r	Radius coordinate
R	Development rate (L/t)
R_G	Grun range given by Eq. (8.12) (L)
R_i	Ion penetration length
R_o	R at M_0
s, s'	Object and image distances in Fig. 8-10
S	Selectivity or the minimum dose at which the dimensional quality of clear and opaque features results; spinning speed (r/min)
t	Time
t_r	Exposure time
T	Tolerance given by Eq. (8.44); temperature
v	Light speed in a transparent material

w	Dose function given by Eq. (8.14)
W	Resolution (minimum feature size)
x	Coordinate perpendicular to resist depth coordinate z
y	Length coordinate in Fig. 8-6
Y	Fractional yield in Eq. (8.45)
z	Distance into resist
Z	Depth of focus in Eqs. (8.23) and (8.24)
Z_1, Z_2	Atomic number of ion and lattice atoms, respectively

Greek letters

α	Included half-angle for a cone in Eq. (8.11) (rad); dissolution order in Eq. (8.32)
β	Standard deviation
β_b	Half-width of backward scattering distribution
β_f	Half-width of forward scattering distribution
β_e	Effective half-width
λ	Wavelength; dose function given by Eq. (8.14)
μ	Absorption coefficient in Eq. (8.21); average number of scission or crosslinking per polymer molecule
ρ	Density
Ω	Solid angle in Eq. (8.10); contrast defined by Eq. (8.34)

Units

A	Ampere
C	Coulomb
E	Energy
L	Length
M	Mass
P	Pressure
t	Time
T	Temperature

PROBLEMS

8.1. The grating formula of Eq. (8.7) is the basis for the spatial frequency of mask lines that can be imaged on a resist with a given light beam. Note that d in the equation is the total length for a combination of clear and opaque lines on the mask and sin Ω can be taken as the numerical aperture. For the first-order (principle) diffraction of interest, $j = 1$. Calculate the minimum length of the repeating clear/opaque lines that can be imaged for a coherent beam of 200 nm wavelength and NA of 0.17. Explain what happens if the desired length is smaller than the minimum. Also explain what happens if it is larger than the minimum. Refer to Fig. 8-17.

8.2. Plot the average axial distribution of energy dissipated and the radial distribution at the resist-substrate interface for a silicon substrate and an e-beam resist for the following cases:

	A	B	C
Incident energy, keV	15	25	25
Resist thickness, μm	1.0	0.5	1.0

Draw conclusions on the effect of the incident energy and resist thickness on the distributions. The electron beam may be assumed to be a spot or a point. Use Table 8.1. For the averaging, use the following:

$$E_v \text{ from Eq. (8.13)} = \int_0^R \frac{rE_v(r, z) \text{ of Eq. (8.15)}\, dr}{R^2/2}$$

where R is 2 times β_b. For simplicity, use ρ of 1 g/cm^3 for the Grun range.

8.3. Calculate the maximum penetration of electron into silicon and compare to the ion range based on Ar^+ for E_o of 20 keV for both. Draw conclusions from the results. Use the atomic density of 10^{22} cm^{-3} and ρ of 2.33 g/cm^3 for silicon.

8.4. X-ray printing is usually done by shadow printing, which is a form of proximity printing. Shadow printing is the typical way of making replicas of masks. Calculate the minimum linewidth that can be projected for a gap of 5 μm and an x-ray of 10 nm wavelength. Determine the energy dissipated at the resist (PMMA)-substrate interface if the resist thickness is 0.5 μm. Assume the incident energy to be 20 mJ/cm^2. Use Fig. 8-14.

8.5. Feder *et al.* (1975) reported a feature of 10 nm using an x-ray of 4.48 nm wavelength. Calculate the gap between the mask and the resist.

8.6. Greeneich (1975) gives the following for the development rate of an electron-beam resist:

$$R \text{ (nm/min)} = \frac{1.046 \times 10^{15}}{M^{3.86}}$$

Calculate the time required to develop the resist for a uniform incident energy of 20 keV. The resist thickness is 0.31 μm. Use the following information:

$$\rho = 1.2 \text{ g/cm}^3 \qquad G = 19 \text{ keV}^{-1} \qquad M_0 = 2 \times 10^5 \qquad D = 5 \times 10^5 \text{ C/cm}^2$$

8.7. The selectivities for some e-beam resists are given below:

$$S = \begin{cases} 2 \times 10^{-5} \text{ (C/cm}^2\text{)} & \text{for PMMA} \\ 4 \times 10^{-7} \text{ (C/cm}^2\text{)} & \text{for COP} \end{cases}$$

Determine the ratio of the minimum features that can be obtained with the resists.

8.8. For the resist considered in Example 8.9, calculate the developed resist width in excess of the clear mask feature for a light beam of 0.3 μm and incident energy of 20 mJ/cm^2.

8.9. For the minimum and maximum exposure time considered in Example 8.4, calculate the corresponding development times for 1-μm thick resist. Use the parameters given in the example.

8.10. For negative e-beam resists, the number of crosslinking events per kiloelectronvolt is around 3; it is usually 19 keV^{-1} for positive resists. For a negative e-beam resist,

Thompson *et al.* (1978) reported the following:

Selectivity (minimum dose) = 4×10^{-7} (C/cm^2)

Dose for 50 percent development in the developed resist thickness versus dose curve = 10×10^{-7} (C/cm^2)

$M_0 = 2.29 \times 10^5$

$\Omega = 1.2$

For an incident energy of 20 keV, calculate the molecular weight at the resist-substrate interface for a resist of 0.6 μm thickness. Do the calculation at the two dose levels given above. Assume the resist density to be 1.2 g/cm^3. For the Grun range, use ρ of 2.33 g/cm^3.

8.11. Suppose only the first term in Eq. (8.46) is taken. Show that the usable throughout P for a given machine, i.e., the fractional number of good circuits in a wafer per unit time, can be written as follows:

$$P = \frac{1}{K' n t_e (1 + A_w D)^n}$$

where t_e is the exposure time. Note that the development time is not included in the formulation.

8.12. Babu and Barouch (1986) arrived at the following implicit solutions of Eqs. (8.38) through (8.40) for positive photoresists:

$$\frac{I_m}{I_0} = \frac{A(1 - M) - B \ln M}{A[1 - \exp(-Dk_i)] + BDk_i} \tag{A}$$

$$\int_{e^{-Dk_i}}^{M} \frac{dy}{y[A(1 - y) - B \ln y]} = z \tag{B}$$

where D is the dose given by $I_0 t$, t being the exposure time. For an ideal photoresist, the absorption coefficient α in Eq. (8.40) should be zero if no inhibitor is present, that is, $B = 0$. For this ideal case (B is usually quite small), the above equations can be manipulated along with Eq. (8.39) to give

$$M(z, t) = \frac{\exp(Az - Dk_i)}{1 + \exp(Az - Dk_i) - \exp(-Dk_i)} \tag{C}$$

which gives the axial inhibitor concentration profile for a given dose. Dill *et al.* (1975b) gave the following parameters for a positive photoresist:

$$A = 0.86\ \mu\text{m}^{-1} \qquad k_1 = 0.018 \text{ cm}^2\text{/mJ} \qquad B = 0.07\ \mu\text{m}^{-1}$$

$$a_1 = 5.63 \qquad a_2 = 7.43 \qquad a_3 = -12.6$$

Plot the inhibitor concentration profiles for the 0.6-μm thick resist for doses of 15, 60, and 240 mJ/cm^2. Set B equal to zero for the plot. Draw conclusions. Calculate the time required to develop the resist for the dose of 60 mJ/cm^2.

8.13. In projection printing photolithography, the lateral intensity distribution imaged on the resist surface is of Gaussian type when the linewidth is smaller than the depth of focus [Eq. (8.24*b*)] according to the rather rigorous simulation obtained by Lin

(1980). Suppose for a 1-μm linewidth that the lateral distribution is given by

$$I = I_i \exp(-bx^2) \tag{A}$$

(*a*) Show that for an incident light flux of 60 mJ/(cm^2·s), the lateral distribution for b of 2 (μm^{-2}) yields

$$I = 47.9 \exp(-2x^2) \quad (\text{mJ/cm}^2) \tag{B}$$

Note that

$$\frac{I_0 w}{2} = I_i \int_0^{\infty} \exp(-2x^2)\, dx \tag{C}$$

where w is the linewidth.

(*b*) For the distribution given by Eq. (B), the equation equivalent to Eq. (C) in Prob. 8.12 is

$$M(z, x) = \frac{\exp(Az - D_i k_i X)}{1 + \exp(Az - D_i k_i X) - \exp(-D_i k_i X)} \tag{D}$$

where X is given by

$$X = \exp(-bx^2)$$

and where D_i is the dose corresponding to I_i. Using the parameters in Prob. 8.12, plot the developed resist profiles similar to the one in Fig. 8-21 as a function of development time for D_i of 60 mJ/cm^2 up to t of 4 s.

8.14. For a polymer to crosslink into an insoluble gel, a certain absorbed energy per unit volume of resist E_r is required so that, on the average, one crosslink per chain is formed. This energy can be related as follows:

$$E_r = \frac{\rho N_A}{G M_0}$$

where G is the average number of the crosslink events per unit energy. If a total of E energy per unit volume is absorbed, the total number of crosslink μ is given by

$$\mu = \frac{E_v}{E_r} = \frac{G M_0 E_v}{\rho N_A}$$

which is Eq. (8.30). Thus, the same μ applies to the negative resists. Since $(1 + \mu)$ number of polymer units with molecular weight of M_0 crosslink into one crosslinked polymer unit of molecular weight of M, one has

$$(\mu + 1)M_0 = M$$

which is Eq. (8.31). The value of μ is around 3 keV^{-1}. Assuming that the crosslinked polymer (gel) becomes insoluble at a dose corresponding to μ of 20, obtain a relationship for α from Eq. (8.32).

8.15. If R is the rate of development in length per time, a mole balance on the decomposed (positive resists) or crosslinked (negative resists) polymer is

$$\frac{dN}{dt} = \frac{RA\rho_M}{M} \tag{A}$$

where N is the number of moles of the polymer, A is the surface area irradiated, ρ_M is the polymer density, and M is the polymer molecular weight. On the other hand, N can also be expressed as

$$N = \rho_M \int_0^z \frac{A(\alpha)\, d\alpha}{M} \tag{B}$$

Derive Eq. (8.33) from the above two relationships.

8.16. When an electron beam is of Gaussian type rather than a spot (delta function), the approximate lateral distribution of the energy dissipated can be obtained by convolution. If β_g is the incident Gaussian half-width, the linear lateral distribution can be expressed (Greeneich, 1980) as

$$E_l(r, z) = \int_0^{2\pi} \int_0^{\infty} r' E_v(r', z) \exp\left(-r - \frac{r'^2}{\beta_g^2}\right) dr'\, d\theta \tag{A}$$

where $E_v(r', z)$ is that given by Eq. (8.15) with the half-widths corrected for the incident beam width as follows:

$$E_v(r, z) = k(z)\left[\exp\left(-\frac{r^2}{\alpha_f^2}\right) + \mu_e\left(\frac{\alpha_f^2}{\alpha_b^2}\right)\exp\left(-\frac{r^2}{\alpha_b^2}\right)\right] \tag{B}$$

where

$$\alpha_f = (\beta_f^2 + \beta_g^2)^{1/2}$$

$$\alpha_b = (\beta_b^2 + \beta_g^2)^{1/2}$$

For the dimensionally correct dissipation energy distribution, i.e., energy/volume as in Eqs. (8.13) and (8.15), one can average as in Prob. 8.2:

$$E_v(z) \text{ of Eq. (8.13)} = \int_0^{2\alpha_b} \frac{E_l\, dr}{4\alpha_b^2} \tag{C}$$

Write procedures for obtaining the values of $k(z)$ and the lateral distribution.

8.17. If I_i is the Fourier transform of the lateral distribution of the incident beam $I_i(x)$, defined by

$$I_i(f) = \int_{-\infty}^{\infty} I_i(x) e^{-ifx}\, dx = F[I_i(x)] \tag{A}$$

the image spatial frequency distribution $I_m(f)$ is given by

$$I_m(f) = I_i(f)\ \text{MTF}\ (f) \tag{B}$$

which follows from the definition of MTF. The MTF for a partially coherent beam (Goodman, 1968) is given by

$$\text{MTF}\ (f) = \frac{2}{\pi}\left\{\cos^{-1}\left(\frac{f}{f_c}\right) - \frac{f}{f_c}\left[1 - \left(\frac{f}{f_c}\right)^2\right]\right\}^{1/2} \tag{C}$$

where the critical spatial frequency f_c is that given by Eq. (8.26). The values of MTF are given in the table below as a function of f/f_c (Lin, 1980):

MTF	f/f_c	MTF	f/f_c
1.0000	0.0000	0.4000	0.4010
0.9000	0.0787	0.3000	0.5852
0.8000	0.1578	0.2000	0.6871
0.7000	0.2378	0.1000	0.8054
0.6000	0.3197	0.0000	1.0000
0.5000	0.4040		

The intensity distribution of the image projected onto the photoresist surface, $I_m(x)$, is obtained by the inverse Fourier transformation of Eq. (B):

$$I_m(x) = \frac{1}{2\pi}\int_{-\infty}^{\infty} I_m(f)e^{ifx}\,df = F^{-1}[I_m(f)] \qquad \text{(D)}$$

For the given incident beam, Eqs. (A) through (D) can be used to numerically calculate $I_m(x)$. Assuming that the incident beam is uniform in its intensity over the 1-μm slit, calculate the projected image intensity at $x = 0.1$ μm, that is, $I_m(0.1)$. For the purpose of calculation, use Δf of $0.1f_c$. The values of NA and λ are 0.45 and 435.8 nm.

REFERENCES

Alles, D. S., F. R. Ashley, A. M. Johnson, and R. L. Townsend: *J. Vac. Sci. Technol.*, vol. 12, p. 1252, 1975.

Babu, S. V., and E. Barouch: *IEEE Elect. Dev. Lett.*, vol. EDL-7, p. 252, 1986.

Ballantyne, J. P.: in G. R. Brewer (ed.), *Electron-Beam Technology in Microelectric Fabrication*, chap. 5, Academic Press, New York, 1980.

Batchelder, T., and J. Piatt: *Solid State Technol.*, p. 211, August 1983.

Bouwhuis, G., and S. Wittekock: *IEEE Elect. Dev.*, vol. ED-26, p. 723, 1979.

Bowden, M. J.: *J. Electrochem. Soc.*, vol. 128, p. 195c, 1981.

Bowmer, T. N., and J. H. O'Donnell: *J. Macromol. Sci.*, vol. A17(A), p. 243, 1982.

Brodie, I., and J. J. Muray: *The Physics of Microfabrication*, Plenum Press, New York, 1982.

Chang, T. H. P.: *J. Vac. Sci. Technol.*, vol. 12, p. 1271, 1975.

Colclaser, R. A.: *Microelectronics Processing and Device Design*, Wiley, New York, 1980.

Cuthbert, J. D.: *Solid State Technol.*, vol. 20, p. 59, August 1977.

Dill, F. H., W. P., Hornberger, P. S. Hauge, and J. M. Shaw: *IEEE Trans. Elect. Dev.*, vol. ED-22, p. 445, 1975a.

———, A. R. Neureuther, J. A. Tuttle, and E. J. Walker: *IEEE Trans. Elect. Dev.*, vol. ED-22, p. 456, 1975b.

Eisberg, R. M., and L. S. Lerner: *Physics: Foundations and Applications*, McGraw-Hill, New York, 1981.

Everhart, T. E., and P. H. Hoff: *J. Appl. Phys.*, vol. 42, p. 5837, 1971.

Feder, R., E. Spiller, and J. Topalian: *J. Vac. Sci. Technol.*, vol. 12, p. 1332, 1975.

Goodman, J. W.: *Introduction to Fourier Optics*, chap. 6, McGraw-Hill, New York, 1968.

Greeneich, J. S.: *J. Electrochem. Soc.*, vol. 122, p. 970, 1975.

———: in G. R. Brewer (ed.), *Electron-Beam Technology in Microelectronic Fabrication*, chap. 2, Academic Press, New York, 1980.

Hatzakis, M.: *J. Vac. Sci. Technol.*, vol. 12, p. 1275, 1975.

Havas, J. R.: *Electrochem. Soc. Extended Abstr.*, vol. 76-2, p. 743, 1976.

Hawryluk, R. J., A. M. Hawryluk, and H. I. Smith: *J. Appl. Phys.*, vol. 45, p. 2551, 1974.

Heidenreich, R. D., J. P. Ballantyne, and L. R. Thompson: *J. Vac. Sci. Technol.*, vol. 12, p. 1284, 1975.

Herriott, D. R., and G. R. Brewer: in G. R. Brewer (ed.), *Electron-Beam Technology in Microelectronic Fabrication*, chap. 3, Academic Press, New York, 1980.

Hershel, R., and C. A. Mack: in N. G. Einspruch (ed.), *VLSI Electronics*, vol. 16, *Lithography for VLSI*, chap. 2, Academic Press, Orlando, 1987.

Herzog, R. F., J. S. Greeneich, T. E. Everhart, and T. Van Duzer: *IEEE Trans. Elect. Dev.*, vol. ED-19, p. 629, 1972.

Jenkins, F., and H. White: *Fundamentals of Optics*, 4th ed., McGraw-Hill, New York, 1976.

Karapiperis, L., I. Adesida, C. A. Lee, and E. D. Wolf: *J. Vac. Sci. Technol.*, vol. 19, p. 1259, 1981.

Kim, D. J., W. G. Oldham, and A. R. Neureuther: *IEEE Trans. Elect. Dev.*, vol. ED-31, p. 1730, 1984.

Kyser, D. F., and N. S. Viswanathan: *IEEE Trans. Elect. Dev.*, vol. 12, p. 1305, 1975.

Lin, B. J.: in R. Newman (ed.), *Fine-Line Lithography*, chap. 2, North-Holland, Amsterdam, 1980.

McGillis, D. A.: in S. M. Sze (ed.), *VLSI Technology*, chap. 7, McGraw-Hill, New York, 1983.

——— and D. L. Fehrs: *IEEE Trans. Elect. Dev.*, vol. ED-22, p. 471, 1975.

Moore, G. E.: Technical Digest International Electrical Development Meeting, pp. 11–13, December 1975.

Moran, J. M., and D. J. Maydan: *J. Vac. Sci. Technol.*, vol. 16, p. 1620, 1979.

Ouano, A. C.: in T. Davidson (ed.), *Polymers in Electronics*, ACS Symposium Series 242, ACS, Washington, 1984.

Pamplone, T. R.: *Solid State Technol.*, p. 115, June 1984.

Parikh, M.: *IBM J. Res. Dev.*, vol. 24, p. 438, 1980.

——— and D. F. Kyser: IBM Research Report RJ2261, 1978.

Price, J. E.: *Proc. IEEE*, vol. 58, p. 1290, 1970.

Saotome, Y., H. Gokam, K. Saiga, M. Suzuki, and Y. Ohniske: *J. Electrochem. Soc.*, vol. 132, p. 909, 1985.

Skinner, J. G.: *Proc. Kodak Interface, '73*, p. 53, 1973.

Spiller, E., and R. Feder: in H. J. Queisser (ed.), *X-Ray Optics*, Springer-Verlag, Berlin, 1977.

Tai, K. L., E. Ong, and R. G. Vadimsky: *Proc. Electrochem. Soc.*, vol. 82 (9), p. 9, 1982.

Thompson, L. F., L. E. Stillwagon, and E. M. Doerries: *J. Vac. Sci. Technol.*, vol. 15, p. 938, 1978.

——— and M. J. Bowden: in L. F. Thompson *et al.* (eds.), *Introduction to Microlithography*, chap. 4, ACS Symposium Series 219, ACS, Washington, 1983.

Trotel, J., and B. Fay: in G. R. Brewer (ed.), *Electron-Beam Technology in Microelectronic Fabrication*, chap. 6, Academic Press, New York, 1980.

Wallmark, J. T.: *IEEE Trans. Elect. Dev.*, vol. ED-26, p. 135, 1979.

Willson, C. G.: in L. F. Thompson *et al.* (eds.), *Introduction to Microlithography*, chap. 3, ACS Symposium Series 219, ACS, Washington, 1983.

Wittels, N. D.: in R. Newman (ed.), *Fine-Line Lithography*, chap. 1, North-Holland, Amsterdam, 1980.

Yoshikawa, A., O. Ochi, H. Nagai, and Y. Mizyshima: *Appl. Phys. Lett.*, vol. 29, p. 677, 1976.